Tuning of vibration absorbers by an effective modal coupling factor

Jan Høgsberg, Boris Lossouarn, Jean-François Deü

International Journal of Mechanical Sciences 268 (2024) 109009

Contents lists available at ScienceDirect

International Journal of Mechanical Sciences

journal homepage: www.elsevier.com/locate/ijmecsci

Tuning of vibration absorbers by an effective modal coupling factor

Jan Høgsberg [a,*], Boris Lossouarn [b], Jean-François Deü [b]

[a] Department of Civil and Mechanical Engineering, Technical University of Denmark, Nils Koppels Allé, building 403, DK-2800, Kongens Lyngby, Denmark
[b] Laboratoire de Mécanique des Structures et des Systèmes Couplés (LMSSC), Conservatoire national des arts et métiers, 292 rue Saint-Martin, 75003 Paris, France

ARTICLE INFO

Keywords:
Structural dynamics
Vibration damping
Tuned vibration absorber
Effective Modal Coupling Factor
Tuned mass and inerter damper
Piezoelectric shunt damping

ABSTRACT

The simplest family of vibration absorbers comprise inertia absorbers, with an inerter in series with a parallel or series dashpot–spring element, and stiffness absorbers, for which inerter and spring are interchanged. Vibration absorbers are tuned to a structure's critical resonance, for which scalar structure-absorber equations are derived from an expansion in vibration modes with the absorber in either a free or clamped state. It is demonstrated that the influence from non-targeted residual modes is consistently represented by an effective modal coupling factor (EMCF), evaluated as the relative difference between free and clamped natural frequencies squared. While closely related to the coupling factor for shunted electromechanical transducers, the use of EMCFs determines an entirely new direction for the tuning of mechanical vibration absorbers on a flexible structure. For inertia and stiffness absorbers, the EMCF represents apparent mass or stiffness ratios that also account for the influence from residual modes. Therefore, analytical tuning expressions can be obtained from the derived modal frequency response functions, as demonstrated for a pole-placement method with the EMCF as a new governing absorber parameter. The accuracy of the proposed absorber tuning is validated by a simple numerical example, which shows that analytical tuning expressions can be used directly for vibration damping of flexible structures, provided that the EMCF is included correctly to compensate for the inherent modal interaction.

1. Introduction

Vibration absorbers are installed or attached to flexible structures to mitigate excessive dynamic response across several engineering scales, from piezoelectric vibration reduction of turbomachinery fans [1] to +100 tons tuned mass dampers and inerters inside modern high-rise buildings [2,3].

In the present study, the vibration absorber introduces a single resonance, which must be optimally synchronized to the single critical vibration mode of the structure. Furthermore, the inherent absorber damping must as well be correctly balanced, to exactly dissipate sufficient vibration energy without restraining the absorber motion too much. In the present contribution, a theoretical framework is proposed for the consistent tuning of the most basic group of vibration absorbers. This involves the introduction of an effective modal coupling factor (EMCF), regularly used for tuning of electromechanical devices, while it represents a novel approach to the design of mechanical vibration absorbers.

The fundamental vibration absorber is the so-called Tuned Mass Damper (TMD), which consists of an auxiliary mass, suspended to the structure by a spring and dashpot placed in parallel. The TMD is initially analysed in detail by Ormondroyd and Den Hartog [4], while tuning formulae are collected by Brock [5] and finally carved in stone as engineering practice in the book of Den Hartog [6]. Various tuning expressions, associated with different optimality conditions, have recently been summarized by Zilletti et al. [7], while the applications of TMDs are thoroughly reviewed by Elias and Matsagar [2]. A recent tuning procedure by Su et al. [8] applies optimality based on a hybrid H_2-H_∞ norm. Furthermore, the influence of structural damping and damper nonlinearities has been accounted for in the tuning expressions by Shum [9].

In smart structures technology, comprising piezoelectric and electromagnetic transducers, vibration absorbers can be realized by electric shunts [10–12]. In piezoelectric vibration control, the use of resonant shunts is ignited by the pioneering papers by Forward [13] and by Hagood and von Flotow [14]. They suggest the use of resistive-inductive (RL) shunts to create a piezoelectric vibration absorber, which mechanically acts as a spring in series with a dashpot-inertia element. Although these piezoelectric absorbers are different from the classic TMD, the same tuning principles may be adopted, as demonstrated in Yamada et al. [15] by the application of Den Hartog's fixed-point tuning for the minimization of various structural response measures. The accuracy of the RL-shunt tuning is further improved by Soltani et al. [16,17], deriving an exact solution for the absolute minimization

* Corresponding author.
E-mail addresses: jahog@dtu.dk (J. Høgsberg), boris.lossouarn@lecnam.net (B. Lossouarn), jean-francois.deu@cnam.fr (J.-F. Deü).

https://doi.org/10.1016/j.ijmecsci.2024.109009
Received 7 September 2023; Received in revised form 2 January 2024; Accepted 2 January 2024
Available online 4 January 2024

of the dynamic amplification curve, while a balanced tuning is proposed by Høgsberg and Krenk in [18–20], applying the equal damping principle by Krenk [21]. The concept of shunted vibration absorbers has also been considered for electromagnetic transducers [11,22,23], which can be scaled to larger structures [24].

The developments in shunted electromechanical absorbers raise the question of how an equivalent inertia that acts on relative motion (elongation) can be realized mechanically. This leads to the introduction of the so-called inerter by Smith [25]. Mechanical inerters convert elongation into rotation, whereby inertance can be generated by low-weight devices, as long as they possess a large rotational inertia. For structural applications, such conversion into rotational inertia has been proposed by Hwang et al. [26] in toggle-brace systems and Ikago et al. [27] for augmented viscous dampers. Tuning expressions for a Tuned Inerter Damper (TID) attached to a dynamic structure are subsequently obtained via its analogy with the TMD by Lazar et al. [28] and extended to a multi-TID configuration by Wen et al. [29]. Tuning expressions for various inerter-based absorber configurations are thoroughly derived in [30,31]. The inerter has also been merged with the TMD to create the so-called Tuned Mass Damper Inerter (TMDI), see Marian and Giaralis [32], where the presence of the inerter can alter the required auxiliary mass from the original TMD to achieve a desired absorber performance. Recently, an improved absorber performance has been reported by Barredo et al. [33] and Chowdhury et al. [34] for inerter-based absorbers with a negative stiffness component. In [33] the inerter-based absorber, with a negative stiffness in parallel to the classic TID, is found to substantially increase the operational damper bandwidth, while in [34] the inclusion of an inerter element with negative stiffness improves the performance of both damping and base-isolation systems.

When tuning the classic TMD, the attainable damping and the degree of response mitigation depend on the mass ratio, which therefore acts as the governing parameter in the expressions for the optimal TMD stiffness and damping. Any coupling with the structure's other (typically higher) modes, not targeted by the TMD, is usually of less importance because the TMD acts on absolute structural motion and is placed optimally where the targeted mode has its maximum deflection. As argued by Krenk and Høgsberg [35], the TID – although model-wise fully equivalent to the TMD – is much more sensitive to modal interaction with other modes because it operates on relative motion of the structure. Thus, if not compensated for, the modal spill-over from other modes will deteriorate the performance of inerter-based absorbers, such as the TID, for which residual mode corrections in [35–37] are derived explicitly by matrix expressions.

For shunted electromechanical absorbers, the approach has been rather different than for the above inertia-based TMD and TID. The authority of an electromechanical shunt absorber is quantified by its ability to convert mechanical energy into electrical energy (and vice versa) in the modal domain. This ability is described by the effective electromechanical coupling factor (EEMCF), which is evaluated in [38–48] by either numerical or experimental means. In most cases the EEMCF is directly determined from the change in the structure's natural frequency squared when switching the transducer electrodes between short- and open-circuit (sc and oc) conditions. The EEMCF serves as a governing stiffness ratio, similar to the mass ratio for the TMD and TID. It is derived by a single-mode approximation in the sc and oc limits, without explicitly accounting for any modal coupling with other (residual) modes. However, this simple evaluation of the governing EEMCF – based on pure single-mode approximations – implicitly includes the influence from residual modes, which is why the derived shunt tuning is commonly sufficiently accurate. The accuracy of the electromechanical coupling in piezoelectric structures has been investigated experimentally by Basak et al. [49] and Kelley et al. [1], reporting some deviations to numerical results because of the inherent difficulty associated with modelling non-ideal bonding conditions.

The present paper proposes a common modelling and tuning approach for a group of simple vibration absorbers, comprising inertia absorbers (such as the TMD and TID) and stiffness absorbers, representing shunted piezoelectric or electromagnetic transducers. Free and clamped limits are defined in Section 2, with governing modal equations derived by an expansion in modes from an eigenvalue problem in either of these two limits. The subsequent truncation of other vibration modes not targeted by the absorber are represented by a modal correction function, which leads to the governing single-mode equations presented in Section 3. It is then demonstrated in Section 4 how this modal correction function is consistently represented by an effective modal coupling factor (EMCF). The main novelty of this paper is based on the introduction of such a coefficient for the tuning of mechanical vibration absorbers. For expansions in free vibration modes, this EMCF replaces the mass ratio for an inertia absorber and the stiffness ratio for a stiffness absorber. When the latter is implemented by a resonantly shunted electromechanical transducer, the EMCF is equivalent to the more classical EEMCF. For the alternative clamped-mode expansion, it is shown that this one-to-one replacement of mass or stiffness ratios by the EMCF is not valid, whereby care must be taken when tuning absorbers by this approach. The absorber tuning is derived in detail for inertia absorbers in Section 5. As summarized in Appendix A, the tuning expressions for the corresponding stiffness absorbers are readily obtained by simply replacing inertia with stiffness. The assessment and comparison of the absorbers is presented in Section 6 for a simple shear-frame structural model, demonstrating the ability of the proposed EMCF to secure accurate tuning.

2. Vibration absorber on flexible structure

Fig. 1 shows a shear-frame structure, representing a generic linear multi-degree-of-freedom (mdof) model, with a simple single-resonance vibration absorber, composed of an inerter placed in series with (a) a parallel or (b) series dashpot–spring element. The isolated inerter depicts these two configurations as inertia absorbers, for which the inertance m governs the damping performance when the stiffness k and viscous coefficient c inside the dashed-blue damper element are calibrated optimally by any preferred tuning procedure. Inertia absorbers mainly comprise mechanical devices, such as the classic tuned mass damper (TMD) [6,21] or the recent tuned inerter damper (TID) [28,31,35,36], shown in Fig. 1(a).

The corresponding stiffness absorbers in Fig. 1(c, d) mainly represent smart or shunted electromechanical devices, such as RL-shunted piezoelectric transducers [14,43–45,50,51] or RC-shunted electromagnetic actuators [11,22,23]. For a piezoelectric transducer, the use of series and parallel RL-shunts is mechanically modelled by the parallel and series stiffness absorbers in Fig. 1(c) and (d), respectively. The isolated spring stiffness k, which in the present context classifies these configurations as stiffness absorbers, represents the intrinsic piezoelectric capacitance, while the dashpot c and inertance m in the damper element (dashed-blue box) are mechanical equivalents to the shunt resistance R and inductance L, respectively.

When introducing "–" for series, "‖" for parallel and "[…]" for the damper element inside the dashed-blue box, the inertia absorbers in Fig. 1(a) and (b) are in the following referred to as m-[c‖k] and m-[c-k], respectively. For the corresponding stiffness absorbers in Fig. 1(c, d), the short notation is then k-[c‖m] for the parallel damper element in (c) and k-[c-m] for the pure series absorber in (d).

By construction, the two series absorbers m-[c-k] and k-[c-m] are mechanically identical. For an idealized single-degree-of-freedom (sdof) structure, any calibration principle will therefore result in identical tuning. However, for a multi-degree-of-freedom (mdof) structure, the representation of the influence from the residual modes that are not targeted by the absorber may be different for the two series absorbers, as demonstrated in connection with the following definition of the effective modal coupling factor (EMCF) in Section 4.

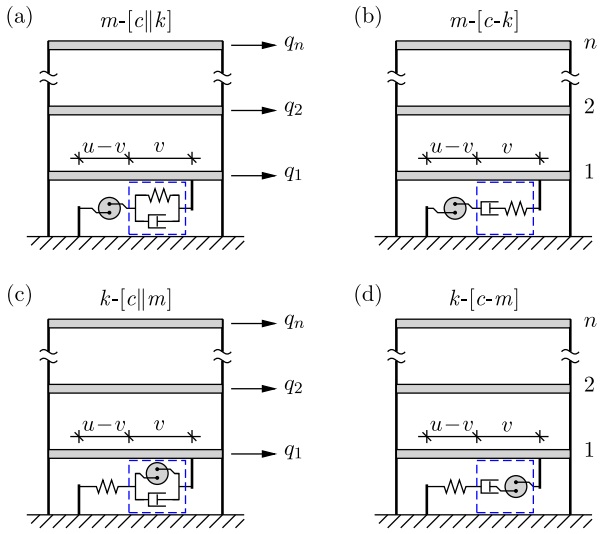

Fig. 1. Shear frame structural model with n floors and absorbers installed between ground and first floor. The horizontal displacements in $\mathbf{q}^T = [q_1, \ldots, q_n]$ represent the model's n dofs. (a, b) shows the inertia absorbers with an isolated inerter in series with (a) a parallel (m-[c||k]) and (b) series (m-[c-k]) spring–dashpot element. (c, d) shows the corresponding stiffness absorbers, composed of an isolated spring and (c) a parallel inerter-dashpot element (k-[c||m]) and (d) a series inerter-dashpot element (k-[c-m]). The elongation of the entire absorber is $u = \mathbf{w}^T\mathbf{q}$, while v represents the elongation of the damper element in the dashed-blue box.

The present section defines the governing equations of motion for the flexible structure, in which the absorber is included by a generic forcing term. The modal expansion is introduced based on either free modes from the undamped eigenvalue problem or the clamped modes, associated with a fully constrained damper elongation. The modal expansions constitute the basis for the derivation of the single-mode models used in the subsequent Section 3.

2.1. Governing equations of motion

The governing structural equations can be expressed in the frequency domain, with variables representing vibration amplitudes as function of the angular frequency ω. For the linear structural model without inherent structural damping, the governing dynamic equation is

$$\left(-\omega^2\mathbf{M} + \mathbf{K}\right)\mathbf{q} + \mathbf{w}f = \mathbf{f}_{\text{ext}} \,, \tag{1}$$

where generalized displacements are contained in $\mathbf{q}$, external loading is represented by $\mathbf{f}_{\text{ext}}$, structural inertia is comprised by the mass matrix $\mathbf{M}$, while the stiffness matrix $\mathbf{K}$ accounts for all restoring effects. The equation of motion (1) contains the absorber force f as the coupling variable to an associated absorber equation, whereby $f = 0$ defines the free structure.

The placement of the absorber on the structure is in (1) determined by a connectivity vector $\mathbf{w}$, which consequently defines

$$u = \mathbf{w}^T\mathbf{q} \tag{2}$$

as the relative structural displacement across the absorber link. The connectivity vector is commonly constructed by the elongation relation in (2). For the very local attachment between ground and first floor in Fig. 1, the connectivity vector becomes $\mathbf{w}^T = [\,1,\, 0,\, \ldots\, 0\,]$ when positive elongation is associated with absorber elongation.

For the absorbers in Fig. 1, the elongation of the damper element in the dashed-blue box is v, whereby the corresponding relative displacement across the absorber element is $u - v$. Hereby, the absorber force f can be expressed by the two relations

$$f = D(\omega)v = G(\omega)(u - v) \,, \tag{3}$$

in which $D(\omega)$ represents the frequency-dependent properties of the damper element, while the absorber function $G(\omega)$ defines the inertia absorbers in Fig. 1(a, b) by $G(\omega) = -\omega^2 m$ and the stiffness absorbers in Fig. 1(c, d) by $G(\omega) = k$.

An alternative form of the equation of motion (1) is obtained by the substitution of the last expression for f in (3), whereby the equation of motion

$$\left(-\omega^2\mathbf{M} + \mathbf{K} + G(\omega)\mathbf{w}\mathbf{w}^T\right)\mathbf{q} - G(\omega)\mathbf{w}v = \mathbf{f}_{\text{ext}} \tag{4}$$

contains the elongation v of the damper element as the coupling variable, while the absorber function $G(\omega)$ either increases the apparent inertia or stiffness at absorber location.

2.2. Limiting eigenvalue problems

Vibration absorbers are commonly tuned to a particular vibration mode. The fundamental free structure equations are obtained for a vanishing absorber force ($f = 0$), which corresponds to $v = u$ from the latter relation in (3). In this free limit, the homogeneous form of the equation of motion (1) yields the commonly used eigenvalue problem

$$\left(\mathbf{K} - \omega_j^2\mathbf{M}\right)\mathbf{u}_j = \mathbf{0} \,, \tag{5}$$

where ω_j is the natural angular frequency of mode j and $\mathbf{u}_j$ is the associated mode shape vector.

Fig. 2(a) shows the free limit of the structure, obtained by a vanishing damper element ($D(\omega) = 0$) in Fig. 1. For inertia absorbers m-[c...], this free eigenvalue problem typically represents the structure without absorber, while for stiffness absorbers k-[c...] it may, for example, correspond to the short-circuit (sc) limit of a piezoelectric transducer. In the following, the structural response $\mathbf{q}$ may be expanded by the free modes $\mathbf{u}_j$,

$$\mathbf{q} = \sum_j \mathbf{u}_j r_j \,, \qquad \mathbf{w}^T\mathbf{u}_j = 1 \,, \tag{6}$$

introducing the modal coordinate r_j. The free vibration modes are conveniently normalized to unity at absorber position by the identity in (6).

The alternative structural Eq. (4) defines the eigenvalue problem

$$\left(\mathbf{K} + G(\bar{\omega}_j)\mathbf{w}\mathbf{w}^T - \bar{\omega}_j^2\mathbf{M}\right)\bar{\mathbf{u}}_j = \mathbf{0} \,, \tag{7}$$

associated with $v = 0$, which corresponds to restraining the elongation of the damper element by $D(\omega) \to \infty$ in (3). The alternative form in (7) is therefore referred to as the clamped eigenvalue problem, with

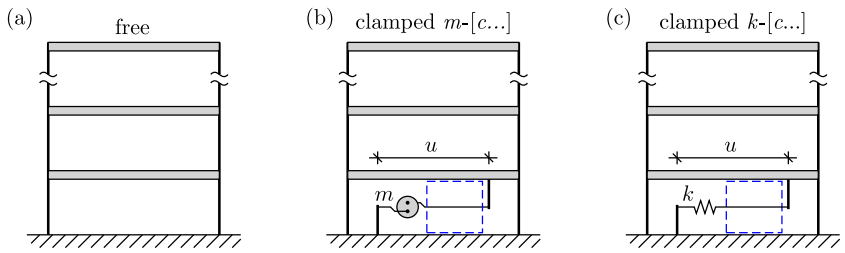

Fig. 2. (a) Free n-floor shear frame structure without absorber ($D = 0$), for which modal properties are presented in Appendix B. (b, c) show the clamped limit for (b) the inertia absorber m-[c...], where m is added to the mass matrix in (10) and (c) the stiffness absorber k-[c...], for which k in (12) is added to the stiffness matrix. For both clamped limits in (b, c), the damper function $D \to \infty$, which implies $v = 0$ in Fig. 1. This is represented by a rigid link through the damper element in the dashed-blue box.

$\bar{\omega}_j$ and $\bar{\mathbf{u}}_j$ as its real-valued natural frequency and mode shape vector, respectively. A clamped-mode expansion of the structural response is expressed as

$$\mathbf{q} = \sum_j \bar{\mathbf{u}}_j \bar{r}_j \ , \qquad \mathbf{w}^T \bar{\mathbf{u}}_j = 1 \ , \tag{8}$$

with respect to the modal coordinate $\bar{r}_j$ and modes scaled to unit deflection at absorber location. For the mechanical TMD or TID, the clamped limit represents the absorber mass or inertance being rigidly attached to the structure, whereas for piezoelectric transducers the clamped limit corresponds to open-circuit (oc) electrodes. The following subsections define the clamped eigenvalue problem (7) for both the inertia and the stiffness absorbers, representing the structural models in Fig. 2(b, c) with an isolated inerter and spring, respectively.

2.2.1. Inertia absorbers: m-[c...]

For the inertia absorbers m-[c...] in Fig. 1(a, b) with an isolated inerter, the absorber function

$$G(\omega) = -\omega^2 m \tag{9}$$

defines the apparent mass m that represents the physical mass in a TMD [6] or the inertance of a TID [28,32]. The free eigenvalue problem (5) is unaffected by the specific absorber type, whereas upon introduction of $G(\omega) = -\omega^2 m$, the clamped eigenvalue problem (7) is written as

$$\left(\mathbf{K} - \bar{\omega}_j^2 \left[\mathbf{M} + m\mathbf{w}\mathbf{w}^T\right]\right) \bar{\mathbf{u}}_j = \mathbf{0} \ . \tag{10}$$

The clamped limit corresponds to a rigid damper element, obtained by the damper function $D(\omega) \to \infty$, whereby the damper elongation $v = 0$, as illustrated in Fig. 2(b) by the rigid link across the dashed-blue box. For the fundamental vibration modes, the clamping of an inertia absorber implies an increase in apparent mass and thus a decrease in natural frequency, i.e. $\bar{\omega}_j \leq \omega_j$.

Although the free-mode expansion in (6), with modes from the eigenvalue problem in (5), is the most used representation for tuning and design of tuned mass and inerter dampers [2,6,7,21,35,36], the clamped eigenvalue problem (10) may in some circumstances be convenient. For the tuned-mass-damper-inerter (TMDI) in [52], the governing equations for a multi-degree-of-freedom structure are naturally derived in the alternative form (4) with the relative absorber deflection v as apparent coupling variable. Furthermore, the clamped-mode expansion has recently been applied by Hoffmeyer and Høgsberg [53] to seemingly better account for the interaction between several TMDs targeting coupled bending–torsion beam vibrations. In practice, the clamped limit is realized by mechanically blocking the stroke of the spring–damper element in Fig. 1(a, b).

2.2.2. Stiffness absorbers: k-[c...]

The stiffness absorber k-[c...] in Fig. 1(c, d) is defined by an isolated spring, represented by the frequency-independent absorber function

$$G(\omega) = k \ . \tag{11}$$

By substitution into (7), the clamped eigenvalue problem

$$\left(\mathbf{K} + k\mathbf{w}\mathbf{w}^T - \bar{\omega}_j^2 \mathbf{M}\right) \bar{\mathbf{u}}_j = \mathbf{0} \tag{12}$$

governs an increase in apparent stiffness because $v = 0$ in Fig. 1(c, d) corresponds to the limit in Fig. 2(c), where the spring k acts directly between the two absorber terminals and thus implies an apparent increase in natural frequency compared to the free-mode solution ($\bar{\omega}_j \geq \omega_j$).

For the tuning and design of piezoelectric shunts, the modal expansion in free vibration modes is the most common approach, see e.g. [14,15,19,20,40,43,50,54,55], for which the coupling term in the structure equation is proportional to the applied voltage. However, the clamped-mode expansion is alternatively applied for shunt-switching by Neubauer et al. [56] during which the electrodes are mostly open, for digital piezoelectric networks in Raze et al. [57] where charge may be the natural control variable or by Deü and Benjeddou [39] for the material modelling of piezoelectric laminates in a composite structure. For piezoelectric transducers, the clamped limit ($D(\omega) \to 0$) corresponds to an infinite impedance, easily realized by fully open-circuit (oc) electrodes. In the material modelling of piezoelectric laminates, the electromechanical coupling is commonly represented by the change in energy between the (free) sc state and the (clamped) oc state [1,49].

3. Target mode equations

When expanding the dynamic response in either free or clamped vibration modes, the presence of an absorber introduces inter-modal coupling, which a tuning procedure to a given mode $j = s$ may account for by including additional correction terms [19,20,35,36,55,58,59] or a feed-through (DC) compensation [60–63]. As demonstrated, a consistent correction for the influence from residual modes will result in different tuning expressions when applying either the free-mode expansion in (6) or the clamped-mode expansion in (8). This section derives the single-mode equations for the damped structure, in which the influence from other (residual) modes is accounted for by a single correction function.

3.1. Inertia absorbers: m-[c...]

For the inertia absorbers m-[c...], this section derives the coupled structure-absorber equations for the targeted vibration mode $j = s$, from both the free and the clamped modal expansion.

3.1.1. Free-mode expansion

The free-mode expansion is introduced by the representation in (6), with r_j as modal coordinate. By substitution of the modal summation into (1), pre-multiplication with $\mathbf{u}_j^T$ gives the modal structure equation

$$\left(k_j - \omega^2 m_j\right) r_j + f = f_j \ , \tag{13}$$

in which the absorber force f appears without scaling because of the unit normalization in (6). The modal mass, modal stiffness and modal load are defined by the expressions

$$m_j = \mathbf{u}_j^T \mathbf{M} \mathbf{u}_j \ , \qquad k_j = \mathbf{u}_j^T \mathbf{K} \mathbf{u}_j \ , \qquad f_j = \mathbf{u}_j^T \mathbf{f}_{\text{ext}} \ . \tag{14}$$

When introducing the modal representation (6) and the absorber function (9) into (3), the associated absorber equation is obtained from (3) as

$$-\omega^2 m v + f + \omega^2 m \sum_j r_j = 0 \ . \tag{15}$$

Hereby, the structure equation (13), absorber equation (15) and damper relation $f = D(\omega)v$ constitute the modal closed-loop system.

From the summation in (15), the targeted term $j = s$ is extracted as it is, while the modal coordinate r_j for the remaining terms ($j \neq s$) is eliminated via the modal structure equation (13) without external loading ($f_j = 0$). Hereby, the absorber equation (15) appears as

$$-\omega^2 m v + \omega^2 m r_s + f - \omega^2 m \sum_{j \neq s} \frac{1}{\omega_j^2 - \omega^2} \frac{f}{m_j} = 0 \ , \tag{16}$$

which is an exact equation for free vibration analysis. The summation of the dynamic flexibility from residual modes is conveniently represented by the frequency dependent function

$$\frac{1}{R_s(\omega)} = \sum_{j \neq s} \frac{1}{\omega_j^2 - \omega^2} \frac{1}{m_j} \ , \tag{17}$$

whereby the single-mode equation for the target mode $j = s$ can be written as

$$-\omega^2 m v + \omega^2 m r_s + \left(1 - \frac{\omega^2 m}{R_s(\omega)}\right) f = 0 \ . \tag{18}$$

The residual mode function R_s will in the subsequent Section 4 be expressed by an effective modal coupling factor (EMCF).

3.1.2. Clamped-mode expansion

For the clamped-mode expansion, the structure equation is obtained by substitution of (8) into (4), introducing $G(\omega) = -\omega^2 m$ and finally pre-multiplying with $\bar{\mathbf{u}}_j^T$. This gives the modal equation

$$\left(\bar{k}_j - \omega^2 \bar{m}_j\right) \bar{r}_j + \omega^2 m v = \bar{f}_j \ , \tag{19}$$

in which the clamped-mode parameters are defined as

$$\bar{m}_j = \bar{\mathbf{u}}_j^T \left[\mathbf{M} + m \mathbf{w}\mathbf{w}^T\right] \bar{\mathbf{u}}_j \ , \qquad \bar{k}_j = \bar{\mathbf{u}}_j^T \mathbf{K} \bar{\mathbf{u}}_j \ , \qquad \bar{f}_j = \bar{\mathbf{u}}_j^T \mathbf{f}_{\text{ext}} \ . \tag{20}$$

For inertia absorbers, the clamping of m to the structure by $v = 0$ seemingly implies $\bar{m}_j > m_j$, although the corresponding change in mode shape may compensate for some of the apparent increase.

The clamped-mode absorber equation becomes identical to the free-mode Eq. (15), when simply replacing the coordinate r_j by $\bar{r}_j$,

$$-\omega^2 m v + f + \omega^2 m \sum_j \bar{r}_j = 0 \ . \tag{21}$$

By the procedure already used in Section 3.1.1 to introduce the residual mode approximation, the clamped-mode absorber equation can be readily expressed as

$$f + \omega^2 m \bar{r}_s - \omega^2 m \left(1 + \frac{\omega^2 m}{\bar{R}_s(\omega)}\right) v = 0 \ , \tag{22}$$

where the residual function

$$\frac{1}{\bar{R}_s(\omega)} = \sum_{j \neq s} \frac{1}{\bar{\omega}_j{}^2 - \omega^2} \frac{1}{\bar{m}_j} \tag{23}$$

is now defined relative to the clamped-mode parameters. In the absorber equation (22), the damper element deflection v is the coupling variable to the structure equation (19), whereby $f = -\omega^2 m \bar{r}_s$ represents the absorber force needed to enforce the clamped limit $v = 0$.

3.2. Stiffness absorbers: k-[c...]

For the stiffness absorbers k-[c...], the coupled modal equations from the previous Section 3.1 for the inertia absorbers can be re-used when replacing inertia $-\omega^2 m$ by stiffness k. Thereby, the correction for residual modes is directly normalized by the governing absorber stiffness.

3.2.1. Free-mode expansion

For the free-mode expansion, the structural modal Eq. (13) is unaffected by the change in absorber type. When replacing absorber inertia $-\omega^2 m$ by stiffness k, the corresponding absorber equation from the free-mode expansion can be directly obtained from (18) as

$$k v - k r_s + \left(1 + \frac{k}{R_s(\omega)}\right) f = 0 \ . \tag{24}$$

Although the present residual mode function R_s is defined as in (17) for the inertia absorber, it will be evaluated differently in Section 4 because the influence from residual modes depends on the absorber type.

3.2.2. Clamped-mode expansion

When replacing $-\omega^2 m$ by k, the clamped-mode structure equation in (19) can be written as

$$\left(\bar{k}_j - \omega^2 \bar{m}_j\right) \bar{r}_j - k v = \bar{f}_j \ , \tag{25}$$

in which modal mass and stiffness are now introduced as

$$\bar{m}_j = \bar{\mathbf{u}}_j^T \mathbf{M} \bar{\mathbf{u}}_j \ , \qquad \bar{k}_j = \bar{\mathbf{u}}_j^T \left[\mathbf{K} + k \mathbf{w}\mathbf{w}^T\right] \bar{\mathbf{u}}_j \ , \tag{26}$$

while modal load $\bar{f}_j$ is defined in (20). Similarly, the clamped-mode stiffness absorber equation

$$f - k \bar{r}_s + k \left(1 - \frac{k}{\bar{R}_s(\omega)}\right) v = 0 \tag{27}$$

has been directly determined by simply replacing $-\omega^2 m$ with k in (22).

4. Effective modal coupling factor

The absorber equations for target mode $j = s$ are derived in the previous Section 3, representing the influence from other modes by the residual functions R_s and $\bar{R}_s$. In the present section, a consistent interpretation of the residual mode correction introduces a so-called effective modal coupling factor (EMCF), which is very similar to the effective electromechanical coupling factor (EEMCF) used in piezoelectric shunt damping [10,12,14].

In the present section, the introduction of the EMCF yields general expressions for the modal frequency response functions (FRFs), which constitute the basis for the absorber tuning in the next Section 5. Furthermore, the derived FRFs for inertia and stiffness absorbers are represented by the equivalent mechanical models in Fig. 3, into which any damper element can be inserted.

4.1. Inertia vibration absorber: m-[c...]

For inertia absorbers m-[c...], the effective absorber size is commonly assessed in terms of a mass ratio and not an EMCF. However, as demonstrated in this section, the EMCF represents an apparent mass ratio that directly includes the influence from residual modes, which may be of particular importance for the tuning of the inerter-based absorbers in Fig. 1(a, b).

4.1.1. Free-mode expansion

From the free-mode expansion, the targeted modal structure equation is given in (13) with index $j = s$. In the free limit ($f = 0$), this modal equation directly defines the free-structure natural frequency

$$\omega_s = \sqrt{\frac{k_s}{m_s}} \tag{28}$$

readily obtained by solving the eigenvalue problem (5). In the opposite clamped limit ($v = 0$), the homogeneous structure equation (13) and absorber equation (18) are combined by eliminating the coupling variable f, which results in a characteristic equation,

$$\omega^4 \frac{m_s m}{R_s(\omega)} - \omega^2 \left(m_s + m + \frac{k_s m}{R_s(\omega)} \right) + k_s = 0 \,, \tag{29}$$

that is seemingly of quadratic order in ω^2. Because the characteristic Eq. (29) represents the clamped limit in Fig. 2(b), it must have $\omega^2 = \bar{\omega}_s^2$ as its single root. For the quadratic Eq. (29) to only have a single root, its quadratic term (proportional to ω^4) must vanish. Thus, for the present inertia absorber, the residual function R_s in (17) must be proportional to ω^2, which suggests the approximation

$$R_s(\omega) \simeq -\omega^2 m_s' \tag{30}$$

that introduces the residual mode inertia m_s'.

The residual function R_s in (30) is substituted into the characteristic Eq. (29), from which the single remaining root directly determines an expression for the clamped natural frequency,

$$\bar{\omega}_s^2 = \omega_s^2 \frac{1}{1 + \mu \dfrac{1}{1 + \dfrac{m}{m_s'}}} \,, \tag{31}$$

which contains the inertia correction ratio m/m_s' and the usual modal mass ratio

$$\mu = \frac{m}{m_s} \,. \tag{32}$$

From (31), the inertia correction ratio can be determined as

$$\frac{m}{m_s'} = \frac{\mu}{\mu_*} - 1 \,, \tag{33}$$

in which the effective modal coupling factor (EMCF) is introduced as

$$\mu_* = \frac{\omega_s^2 - \bar{\omega}_s^2}{\bar{\omega}_s^2} \,. \tag{34}$$

It is seen from (33) that the EMCF μ_* represents an apparent mass ratio, which recovers the actual mass ratio ($\mu_* = \mu$) for vanishing residual mode correction ($m/m_s' = 0$). Thus, in the following, the EMCF is used for absorber tuning because it directly accounts for the influence from residual modes ($j \neq s$). The free and clamped natural frequencies in (34) can be determined either numerically as the solution to the eigenvalue problems in (5) and (10) or experimentally for the actual structure with the absorber in its two limits.

When introducing R_s from (30) and then eliminating m/m_s' by (33), the final form of the absorber equation (18) can be written as

$$-\omega^2 m \frac{\mu_*}{\mu} v + f + \omega^2 m \frac{\mu_*}{\mu} r_s = 0 \,, \tag{35}$$

with a modified absorber mass $m\mu_*/\mu$. By first introducing $f = D(\omega)v$ and then eliminating v by (35), the modal structure equation (13) will for $j = s$ determine the frequency response function (FRF),

$$\frac{r_s k_s}{f_s} = \frac{-\dfrac{\omega^2}{\omega_s^2}\mu_* + D(\omega)/k_s}{\left(1 - \dfrac{\omega^2}{\omega_s^2}\right)\left(-\dfrac{\omega^2}{\omega_s^2}\mu_* + D(\omega)/k_s\right) - \dfrac{\omega^2}{\omega_s^2}\mu_* D(\omega)/k_s} \,, \tag{36}$$

for the modal coordinate r_s. The normalization of ω by the free-mode frequency ω_s entirely cancels the mass ratio μ, whereby the EMCF μ_* from (34) constitutes the governing absorber mass ratio.

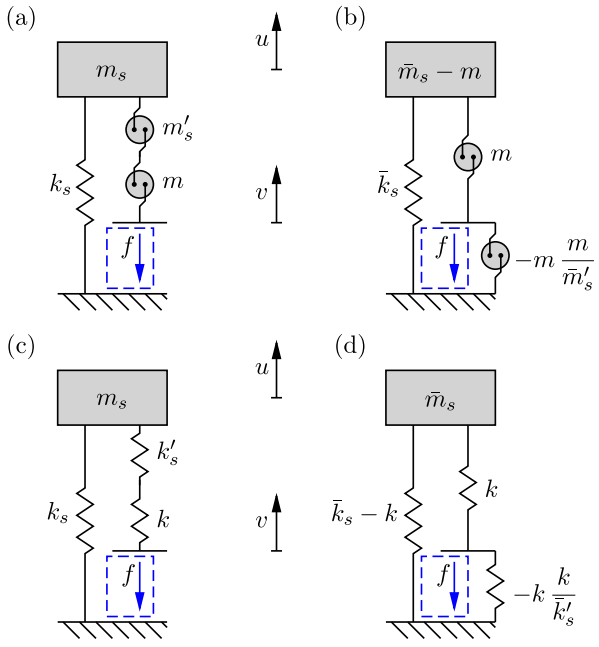

Fig. 3. Equivalent sdof models with (a, b) inertia and (c, d) stiffness absorbers from (a, c) the free- or (b, d) the clamped-mode expansion. Any damper relation $f = D(\omega)v$ can be included in the dashed-blue box. Analytical tuning expressions derived for these four sdof-models can be used for flexible structures because the residual mode components (m_s', k_s', $\bar{m}_s'$ or $\bar{k}_s'$) account for modal interaction.

It can be shown that the mechanical model in Fig. 3(a) corresponds to the FRF in (36) when $f = D(\omega)v$ and f_s acts on the main mass m_s. Thus, for the present free-mode expansion, the residual inertia m_s' in (33) is placed directly in series with the inertance m, as shown in Fig. 3(a). In the free limit, the dashed-blue damper element in Fig. 3(a) is unable to transfer force, whereby the mechanical model recovers the undamped structural oscillator for mode $j = s$. In the clamped limit, the damper element becomes rigid, whereby the inertia increases to $(1+\mu_*)m_s$ with the EMCF determined by (34). Both limits of the damper element are readily verified by $D(\omega) = 0$ and $D(\omega) \to \infty$ in the FRF (36).

4.1.2. Clamped-mode expansion

In the clamped-mode limit ($v = 0$) the associated structural Eq. (19) determines the natural frequency

$$\bar{\omega}_s = \sqrt{\frac{\bar{k}_s}{\bar{m}_s}} \tag{37}$$

for the structural model in Fig. 2(b) with the additional inerter.

In the opposite free limit ($f = 0$), representing the structure without absorber in Fig. 2(a), the coupling variable v is eliminated between (22) and (19), whereby the modal Eq. (19) for $j = s$ determines the reduced characteristic equation

$$-\omega^4 \frac{\bar{m}_s m}{\bar{R}_s(\omega)} - \omega^2 \left(\bar{m}_s - m - \frac{\bar{k}_s m}{\bar{R}_s(\omega)} \right) + \bar{k}_s = 0 \,, \tag{38}$$

which must have $\omega = \omega_s$ as its only solution for the targeted mode. As for the previous free-mode expansion, this single-solution requirement implies that $\bar{R}_s(\omega) \propto \omega^2$, which yields the approximation

$$\bar{R}_s(\omega) \simeq -\omega^2 \bar{m}_s' \,, \tag{39}$$

introducing the clamped-mode residual inertia $\bar{m}_s'$. By substituting this expression for the residual mode function, the solution to (38) determines the free natural frequency as

$$\omega_s^2 = \bar{\omega}_s^2 \frac{1}{1 - \bar{\mu} \dfrac{1}{1 - \dfrac{m}{\bar{m}_s'}}} \,, \tag{40}$$

introducing the clamped-mode mass ratio

$$\bar{\mu} = \frac{m}{\bar{m}_s} \,. \tag{41}$$

From (40) the residual mode mass ratio

$$\frac{m}{\bar{m}'_s} = 1 - \frac{\bar{\mu}}{\bar{\mu}_*} \tag{42}$$

defines the clamped-mode EMCF

$$\bar{\mu}_* = \frac{\omega_s^2 - \bar{\omega}_s^2}{\omega_s^2} \tag{43}$$

so that $\bar{\mu}_* = \bar{\mu}$ when $m/\bar{m}'_s = 0$. By the elimination of $\bar{\omega}_s^2/\omega_s^2$ between (34) and (43), it is obtained that $\bar{\mu}_* < \mu_*$, which demonstrates that the effective absorber mass is smaller when using the clamped-mode expansion.

The absorber equation (22) is reduced by introducing (39) and then eliminating $m/\bar{m}'_s$ from (42),

$$-\omega^2 m \frac{\bar{\mu}}{\bar{\mu}_*} v + f + \omega^2 m \bar{r}_s = 0 \,. \tag{44}$$

When substituting $f = D(\omega)v$ into (44) and then using this absorber equation to eliminate v in (19), the resulting structure equation determines the modal FRF as

$$\frac{\bar{r}_s \bar{k}_s}{\bar{f}_s} = \frac{-\dfrac{\omega^2}{\bar{\omega}_s^2}\dfrac{\bar{\mu}^2}{\bar{\mu}_*} + D(\omega)/\bar{k}_s}{\left(1 - \dfrac{\omega^2}{\bar{\omega}_s^2}\right)\left(-\dfrac{\omega^2}{\bar{\omega}_s^2}\dfrac{\bar{\mu}^2}{\bar{\mu}_*} + D(\omega)/\bar{k}_s\right) - \left(\dfrac{\omega^2}{\bar{\omega}_s^2}\bar{\mu}\right)^2} \,. \tag{45}$$

In this clamped-mode FRF, the mass ratio $\bar{\mu}$ is not uniquely replaced by the EMCF, whereby both $\bar{\mu}$ and $\bar{\mu}_*$ will appear in the subsequent tuning expressions, see [53].

Fig. 3(b) shows the equivalent mechanical model for the clamped-mode FRF in (45). The structural mass $\bar{m}_s$ is reduced by m because the modal mass in (20) implicitly contains the auxiliary absorber mass. In the clamped limit, the mass m from inerter and auxiliary mass cancel, recovering $\bar{m}_s$ as modal mass. In the opposite free limit, the two inerters in series represent the inertia relation (42) that defines the residual mode correction. Thus, for the clamped mechanical model in Fig. 3(b), the residual mode correction is consistently introduced by the negative inertance in parallel to the (dashed-blue) damper element, whereby $\bar{m}'_s$ cannot be merged with m to constitute an effective absorber inertance. Consequently, the FRF in (45) contains both the modal mass ratio $\bar{\mu}$ and the EMCF $\bar{\mu}_*$.

4.2. Stiffness vibration absorber: k-[c...]

The use of an EMCF is common practice in design and tuning of shunted piezoelectric transducers [14,38,39,41,43–48,64]. Therefore, the present section only provides a brief summary of how the EMCF consistently governs the modal equations for a structure with a stiffness absorber, see Fig. 1(c, d). Furthermore, the previous expressions for the inertia absorber in Section 4.1 are directly applicable for the present stiffness absorber when replacing $-\omega^2 m$ with k.

4.2.1. Free-mode expansion

For the stiffness absorber, the clamped limit is shown in Fig. 2(c) and the single natural frequency $\omega = \bar{\omega}_s$ is governed by the eigenvalue problem (12) with an additional stiffness term. Therefore, the single frequency solution requires that the correction function $R_s = k'_s$ in (24), with k'_s being a stiffness component induced by residual modes. The corresponding stiffness correction ratio k/k'_s is then represented by the EMCF

$$\kappa_* = \frac{\bar{\omega}_s^2 - \omega_s^2}{\omega_s^2} \,, \tag{46}$$

which appears as the apparent stiffness ratio that retains the modal stiffness ratio

$$\kappa = \frac{k}{k_s} \tag{47}$$

for vanishing residual mode correction ($k/k'_s = 0$). The free-mode FRF for the present stiffness absorber can finally be written as

$$\frac{r_s k_s}{f_s} = \frac{\kappa_* + D(\omega)/k_s}{\left(1 - \dfrac{\omega^2}{\omega_s^2}\right)\left(\kappa_* + D(\omega)/k_s\right) + \kappa_* D(\omega)/k_s} \tag{48}$$

by simply replacing $-\mu_*\omega^2/\omega_s^2$ in (36) with κ_*, which thereby acts as a unified stiffness ratio.

Fig. 3(c) shows the equivalent mechanical model for the FRF in (48). As for the previous free-mode model in Fig. 3(a), the residual mode correction element k'_s is directly combined with the governing absorber component k to yield the EMCF κ_* as the single governing absorber parameter. For piezoelectric shunt damping, the natural frequencies ω_s and $\bar{\omega}_s$ refer to sc and oc limits, whereby κ_* in (46) represents the effective electromechanical coupling factor (EEMCF) used in e.g. [14,50,65].

4.2.2. Clamped-mode expansion

For the clamped-mode expansion, the residual function in (27) must satisfy the form $\bar{R}_s = \bar{k}'_s$ for the associated characteristic equation to only have a single solution $\omega = \omega_s$ in the free limit, shown in Fig. 2(a). The residual mode stiffness ratio is then eliminated in terms of the EMCF

$$\bar{\kappa}_* = \frac{\bar{\omega}_s^2 - \omega_s^2}{\bar{\omega}_s^2} \,, \tag{49}$$

which for $k/\bar{k}'_s \to 0$ recovers the classic clamped-mode stiffness ratio

$$\bar{\kappa} = \frac{k}{\bar{k}_s} \,. \tag{50}$$

The associated frequency response function is obtained by combining the absorber equation (27) and the modal structure equation (25). When eliminating the stiffness correction by the EMCF, the final form of the FRF can be written as

$$\frac{\bar{r}_s \bar{k}_s}{\bar{f}_s} = \frac{\left(\dfrac{\bar{\kappa}^2}{\bar{\kappa}_*} + D(\omega)/\bar{k}_s\right)}{\left(1 - \dfrac{\omega^2}{\bar{\omega}_s^2}\right)\left(\dfrac{\bar{\kappa}^2}{\bar{\kappa}_*} + D(\omega)/\bar{k}_s\right) - \bar{\kappa}^2} \,, \tag{51}$$

which corresponds to (45) when replacing inertia by stiffness. The FRF indicates that both $\bar{\kappa}$ and $\bar{\kappa}_*$ will appear in a subsequent absorber tuning from a clamped-mode expansion.

As the equivalent model in Fig. 3(d) is obtained from the corresponding inertia absorber model in Fig. 3(b) by interchanging inertance and stiffness, the clamped-mode stiffness $\bar{k}_s$ is now reduced by k, while a negative residual stiffness is placed in parallel with the damper element (dashed-blue box). Therefore, the residual mode component $\bar{k}'_s$ and the absorber stiffness k cannot be combined to a single governing absorber parameter, leaving the FRF in (51) with both the stiffness ratio $\bar{\kappa}$ and the EMCF $\bar{\kappa}_*$. In relation to piezoelectric shunt damping, it may be noted that the tuning in Appendix A based on oc (clamped) modal parameters must consistently use the EMCF in (49), which is normalized by the oc natural frequency ($\bar{\omega}_s^2$).

5. Absorber tuning

Most tuning procedures use the modal frequency response functions (FRFs) derived in Section 4 to either target a minimum vibration amplitude or maximum attainable damping. Various tuning expressions for typical absorbers are derived or summarized in [7,14–16,18,21,31,46,50,66]. This section applies the pole-placement tuning by Krenk [21,

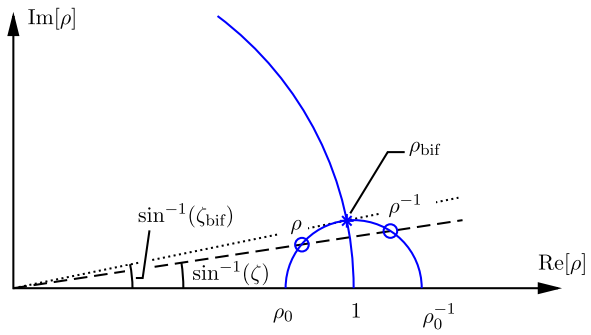

Fig. 4. Idealized root locus diagram for normalized frequency ρ. The single-frequency solution on the real-valued axis at $\rho = 1$ defines the unit-circle backbone trajectory, while the inverse point frequencies $\rho = \rho_0$ and $\rho = \rho_0^{-1}$ describe the semi-circular path that defines a bifurcation point at its intersection with the backbone trajectory. The maximum damping ratio ζ_{bif} occurs for $\rho = \rho_{\text{bif}}$ at the bifurcation ($*$), while the desired tuning places the two inverse poles ρ and ρ^{-1} on the semi-circular path ($\circ$), sufficiently below the bifurcation point to avoid amplitude amplification in the frequency response analysis.

Table 1
Tuning expressions for inertia (top) and stiffness (bottom) absorbers.

m-[*c*‖*k*]		*m*-[*c*-*k*]	
Free	Clamped	Free	Clamped
$\kappa = \dfrac{\mu_*}{(1+\mu_*)^2}$	$\bar{\kappa} = \bar{\mu}^2 \dfrac{1-\bar{\mu}_*}{\bar{\mu}_*}$	$\kappa = \mu_*$	$\bar{\kappa} = \dfrac{\bar{\mu}^2}{\bar{\mu}_*(1-\bar{\mu}_*)}$
$\beta = \sqrt{2\dfrac{\mu_*^3}{(1+\mu_*)^3}}$	$\bar{\beta} = \bar{\mu}^2\sqrt{2\dfrac{1-\bar{\mu}_*}{\bar{\mu}_*}}$	$\beta = \sqrt{\frac{1}{2}\mu_*}$	$\bar{\beta} = \bar{\mu}^2\sqrt{\dfrac{1}{2\bar{\mu}_*^3}}$
k-[*c*‖*m*]		*k*-[*c*-*m*]	
Free	Clamped	Free	Clamped
$\mu = \dfrac{\kappa_*}{(1+\kappa_*)^2}$	$\bar{\mu} = \bar{\kappa}^2 \dfrac{1-\bar{\kappa}_*}{\bar{\kappa}_*}$	$\mu = \kappa_*$	$\bar{\kappa} = \dfrac{\bar{\kappa}^2}{\bar{\kappa}_*(1-\bar{\kappa}_*)}$
$\beta = \sqrt{2\dfrac{\kappa_*^3}{(1+\kappa_*)^3}}$	$\bar{\beta} = \bar{\kappa}^2\sqrt{2\dfrac{1-\bar{\kappa}_*}{\bar{\kappa}_*}}$	$\beta = \sqrt{\frac{1}{2}\kappa_*}$	$\bar{\beta} = \bar{\kappa}^2\sqrt{\dfrac{1}{2\bar{\kappa}_*^3}}$

67], which secures equal damping in the two vibration forms associated with the targeted mode $j = s$. The tuning is only presented in detail for inertia absorbers, while the expressions for the stiffness absorbers in Appendix A are obtained by interchanging inertia and stiffness. The full family of tuning expressions derived in this section is subsequently summarized in Table 1.

5.1. Bifurcation point equation

The desired root-locus diagram in Fig. 4 is governed by two limits with respect to the viscous coefficient c as gain parameter. For each absorber, a non-dimensional frequency ρ is initially defined so that $\rho = 1$ in the single-root limit at $c \to \infty$ for a parallel damper element (… -[c‖ …]) and $c \to 0$ for a series damper element (… -[c-…]). In the opposite limits of c, the targeted mode $j = s$ is governed by two roots, which for the desired absorber frequency tuning are inverse values ($\rho = \rho_0$ and $1/\rho_0$) on the real axis in Fig. 4. Hereby the root trajectories in the complex plane meet at the bifurcation point $\rho = \rho_{\text{bif}}$, depicted by the asterisk in Fig. 4.

The damping ratio ζ_{bif} at the bifurcation point represents the maximum attainable damping, represented by the dotted line in Fig. 4. However, as demonstrated for both the tuned mass damper [21] and piezoelectric shunt damping [14], the bifurcation point tuning creates an amplified response amplitude. Therefore, a proper root placement is slightly below the bifurcation point on the outer semi-circular paths, as indicated in Fig. 4 by the two circles on the same dashed line.

The desired root locus diagram in Fig. 4 relies entirely on the existence of the bifurcation point $\rho = \rho_{\text{bif}}$, which guarantees that two roots ($\circ$) on the semi-circular trajectories have equal damping ratios ζ. A generic characteristic equation that governs a bifurcation point $\rho_{\text{bif}} = a + ib$ can be constructed as

$$(\rho - \rho_{\text{bif}})^2(\rho + \bar{\rho}_{\text{bif}})^2 = 0 \,, \tag{52}$$

with $\bar{\rho}_{\text{bif}} = a - ib$ being its complex conjugate.

As the bifurcation point resides on the unit circle, the two roots are normalized by $|\rho_{\text{bif}}|^2 = a^2 + b^2 = 1$, whereby the real-part is conveniently eliminated by $a = \sqrt{1-b^2}$, while the imaginary part then directly defines a damping ratio,

$$\zeta_{\text{bif}} = \frac{\text{Im}[\rho_{\text{bif}}]}{|\rho_{\text{bif}}|} = b \,, \tag{53}$$

at the bifurcation point. Thus, the quartic equation (52) can be expressed as

$$\rho^4 - \rho^2\left(2 + (2\zeta_{\text{bif}})^2\right) + 1 + 2i\rho(2\zeta_{\text{bif}})\left(-\rho^2 + 1\right) = 0 \,. \tag{54}$$

In the following, a given absorber is tuned by direct comparison of its characteristic equation with this generic polynomial in (54). Further details about this balanced or equal modal damping calibration can be obtained in [18,19,21,67].

5.2. Parallel inertia absorber: *m*-[*c*‖*k*]

For the parallel inertia absorber *m*-[*c*‖*k*] in Fig. 1(a), the damper element inside the dashed-blue box is defined by the damper function

$$D(\omega) = k + i\omega c \,, \tag{55}$$

which represents both a TMD [6,21] and a TID [28,31]. This section derives the tuning expressions for this absorber from both a free- and clamped-mode expansion, using the EMCF to directly account for the influence from residual vibration modes.

5.2.1. Free-mode expansion

From a free-mode expansion, the FRF is obtained by substitution of (55) into (36). The reference frequency ρ is initially determined in

the single-root limit, which for the parallel damper element in (55) is reached by $c \to \infty$, in which case the FRF reduces to

$$\frac{r_s k_s}{f_s} = \frac{1}{1 - \dfrac{\omega^2}{\omega_s^2}(1+\mu_*)} \,. \tag{56}$$

As the reference frequency ρ must be unity in this single-root limit, it follows from (56) that

$$\rho = \frac{\omega}{\omega_s}\sqrt{1+\mu_*} \,. \tag{57}$$

When introducing ρ from (57), the FRF in (36) can be written in normalized form as

$$\frac{r_s k_s}{f_s} = \frac{(1+\mu_*)\left(-\rho^2\mu_* + i\rho\beta\sqrt{1+\mu_*} + \kappa(1+\mu_*)\right)}{\left(1+\mu_*-\rho^2\right)\left(-\rho^2\mu_* + i\rho\beta\sqrt{1+\mu_*} + \kappa(1+\mu_*)\right)\ldots} \tag{58}$$

$$\frac{}{\ldots - \rho^2\mu_*\left(\kappa(1+\mu_*) + i\rho\beta\sqrt{1+\mu_*}\right)} \,,$$

with the stiffness ratio κ defined in (47), while the damper ratio

$$\beta = \frac{c}{\sqrt{m_s k_s}} \tag{59}$$

is normalized by the geometric mean of modal mass m_s and stiffness k_s.

The FRF denominator in (58) determines the characteristic equation

$$\rho^4 - \rho^2\left(1+\mu_*+(1+\mu_*)^2\frac{\kappa}{\mu_*}\right) + (1+\mu_*)^2\frac{\kappa}{\mu_*}\ldots$$
$$\ldots + i\rho\left(\sqrt{1+\mu_*}\right)^3\frac{\beta}{\mu_*}\left(-\rho^2+1\right) = 0 \,. \tag{60}$$

A one-to-one comparison with the generic Eq. (54) then gives the tuned absorber parameters. Initially, the stiffness ratio

$$\kappa = \frac{\mu_*}{(1+\mu_*)^2} \tag{61}$$

is found by comparison of the constant terms in (60) and (54). This expression corresponds to the absorber frequency tuning in [6,7,21] when the EMCF μ_* is replaced by the mass ratio μ. Comparison of the quadratic terms then determines the damping ratio

$$\zeta_{\text{bif}} = \frac{1}{2}\sqrt{\mu_*} \tag{62}$$

at the bifurcation point, which shows that the level of attainable damping is entirely governed by the EMCF. Substitution of ζ_{bif} into the common odd-term coefficient in (54), followed by comparison with (60), gives the absorber damper ratio

$$\beta_{\text{bif}} = 2\sqrt{\frac{\mu_*^3}{(1+\mu_*)^3}} \,, \tag{63}$$

associated with the bifurcation point. To avoid the undesirable response amplification at the bifurcation point, the damper ratio is reduced by division with $\sqrt{2}$,

$$\beta = \frac{1}{\sqrt{2}}\beta_{\text{bif}} = \sqrt{2\,\frac{\mu_*^3}{(1+\mu_*)^3}} \,, \tag{64}$$

which places the roots at the circles in Fig. 4. The damper tuning in (64) is equivalent to the absorber damping ratio proposed in [21,67].

For a single-mode structure, the blue-solid curves in Fig. 5 depict the root locus diagram (a) and the dynamic magnification factor |FRF| (b) obtained from the FRF in (58) with $\mu_* = 0.02$ and the absorber parameters determined by (61) and (64). It is seen in Fig. 5(a) that the complex roots follow trajectories for increasing β that meet at a bifurcation point, and then branch off along the desired unit circle. For the |FRF| in Fig. 5(b), the two (blue) peaks are almost ideally levelled into a flat plateau around the targeted resonance. The specific root locus in Fig. 5(a) is exactly identical to those obtained for the other absorbers, while the |FRF| may differ, as indicated by the red-dashed curve in Fig. 5(b), which represents the free-mode tuning of the parallel stiffness absorber in Appendix A.1.1. It is seen that the red-dashed curve for the stiffness absorber is slightly inclined, corresponding to a flat plateau for the acceleration amplitude $\rho^2|r_s|$ in Fig. 5(d). The frequency amplitude curves for the parallel inertia and stiffness absorber are almost symmetrical for the velocity amplitude $\rho|r_s|$ in Fig. 5(c).

Fig. 6 shows the vibration amplitudes for the dynamic absorber elongation. In Fig. 6(a) the elongation v of the spring–dashpot damper element (dashed-blue box) in Fig. 1(a) is obtained from the absorber equation (35) as

$$\frac{v k_s}{f_s} = \frac{-\rho^2\dfrac{\mu_*}{1+\mu_*}}{-\rho^2\dfrac{\mu_*}{1+\mu_*} + D(\rho)/k_s}\,\frac{r_s k_s}{f_s} \,, \tag{65}$$

with respect to the FRF in (58) and with $D(\rho)$ in (55) expressed in terms of the non-dimensional frequency ρ in (57). For the parallel inertia absorber (blue-solid), the tuning of β in (64) yields a perfectly flat plateau for $|v|$ in Fig. 6(a), an optimal property already discussed by Krenk [21] for the TMD. Fig. 6(b) shows the corresponding elongation of the inerter element, obtained from (3) as

$$\frac{(u-v)k_s}{f_s} = \frac{D(\rho)}{G(\rho)}\,\frac{v k_s}{f_s} \,, \tag{66}$$

with $D(\rho)$ from (55) and $G(\rho)/k_s = -\rho^2\mu/(1+\mu_*)$ expressed in terms of the non-dimensional frequency ρ. The (blue-solid) amplitude curve for the inerter elongation $|u-v|$ exhibits a clear inclination, which becomes flat for the corresponding acceleration amplitude $\rho^2|u-v|$.

The red-dashed curves in Fig. 6 depict the absorber elongations for the corresponding parallel stiffness absorber k-$[c\|m]$ with $\kappa_* = 0.02$, see Appendix A.1.1. It is seen that they are qualitatively interchanged when compared to the present inertia absorber (blue-solid), since the inerter and spring elements are simply placed oppositely. The very small discrepancies that still remain occur because of the influence from the absorber dashpot. For the stiffness absorber k-$[c\|m]$, it is therefore seen that the red-dashed curve becomes ideally flat for $u-v$ in Fig. 6(b), which represents the elongation of the spring in Fig. 1(c).

5.2.2. Clamped-mode expansion

From the clamped-mode expansion, the frequency response function (FRF) is obtained by substitution of the damper function $D(\omega)$ from (55) into (45). For parallel absorbers, the single-root limit is attained by $c \to \infty$, in which case the FRF identifies

$$\bar{\rho} = \frac{\omega}{\bar{\omega}_s} \tag{67}$$

as the non-dimensional frequency that secures $\bar{\rho} = 1$. When introducing $\bar{\rho}$, the full FRF can be written as

$$\frac{\bar{r}_s\bar{k}_s}{\bar{f}_s} = \frac{-\bar{\rho}^2\dfrac{\bar{\mu}^2}{\bar{\mu}_*} + i\bar{\rho}\bar{\beta} + \bar{\kappa}}{\left(1-\bar{\rho}^2\right)\left(-\bar{\rho}^2\dfrac{\bar{\mu}^2}{\bar{\mu}_*} + i\bar{\rho}\bar{\beta} + \bar{\kappa}\right) - \left(\bar{\rho}^2\bar{\mu}\right)^2} \,, \tag{68}$$

with modal parameters $\bar{\mu}$ and $\bar{\kappa}$ defined respectively in (41) and (50), while the clamped-mode damper ratio is defined similarly to (59) as

$$\bar{\beta} = \frac{c}{\sqrt{\bar{m}_s\bar{k}_s}} \,. \tag{69}$$

From the FRF denominator in (68), the characteristic equation can be expressed as

$$\bar{\rho}^4 - \bar{\rho}^2\frac{\bar{\kappa}+\dfrac{\bar{\mu}^2}{\bar{\mu}_*}}{\dfrac{\bar{\mu}^2}{\bar{\mu}_*} - \bar{\mu}^2} + \frac{\bar{\kappa}}{\dfrac{\bar{\mu}^2}{\bar{\mu}_*} - \bar{\mu}^2} + i\bar{\rho}\frac{\bar{\beta}}{\dfrac{\bar{\mu}^2}{\bar{\mu}_*} - \bar{\mu}^2}\left(-\bar{\rho}^2+1\right) = 0 \,. \tag{70}$$

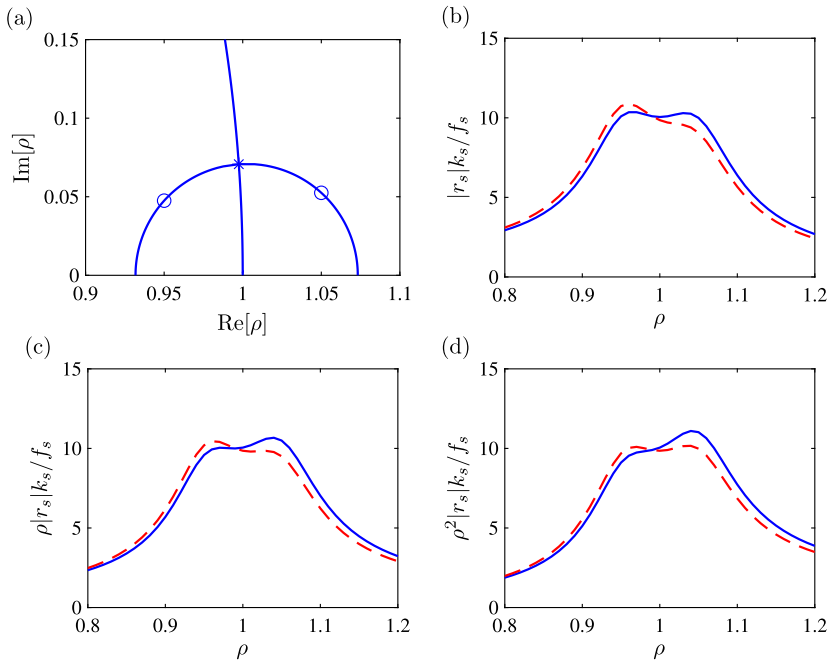

Fig. 5. (a) Root locus diagram obtained by solving the characteristic Eq. (60) for optimal κ in (61) and β varying from 0 to ∞. Optimal damper tuning (64) at circles (∘) and bifurcation tuning (63) at asterisk (∗). (b-d) |FRF| from free-mode expansion: Parallel inertia absorber (m-[c‖k]) with $\mu_* = 0.02$ (blue-solid ——) and parallel stiffness absorber (k-[c‖m]) with $\kappa_* = 0.02$ (red-dashed – –). (b) Modal displacement amplitude $|r_s|$, (c) modal velocity amplitude $\rho|r_s|$ and (d) modal acceleration amplitude $\rho^2|r_s|$. The modal amplitude is normalized by the static deflection f_s/k_s and ρ is defined in (57).

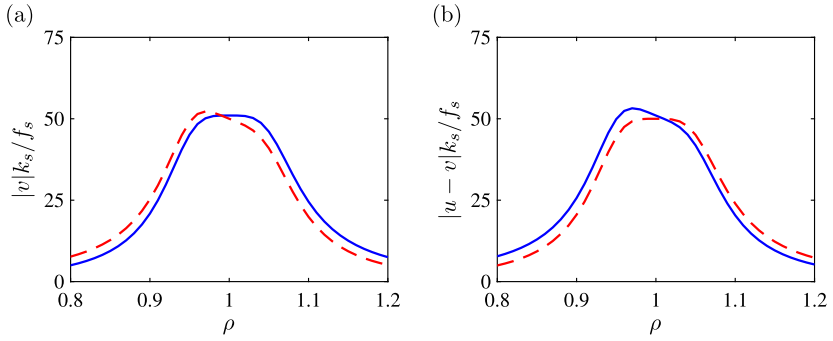

Fig. 6. |FRF| from free-mode expansion: Parallel inertia absorber (m-[c‖k]) with $\mu_* = 0.02$ (blue-solid ——) and parallel stiffness absorber (k-[c‖m]) with $\kappa_* = 0.02$ (red-dashed – –). (a) Damper element amplitude $|v|$ and (b) absorber element amplitude $|u - v|$. Modal amplitude is normalized by the static deflection f_s/k_s.

Comparison of the constant terms in Eqs. (70) and (54) determines the optimal absorber stiffness ratio

$$\bar{\kappa} = \frac{\bar{\mu}^2}{\bar{\mu}_*} - \bar{\mu}^2 = \bar{\mu}^2 \frac{1 - \bar{\mu}_*}{\bar{\mu}_*} \,, \tag{71}$$

while subsequent comparison of the quadratic terms provides the bifurcation-point damping ratio

$$\zeta_{\text{bif}} = \frac{1}{2}\sqrt{\frac{\bar{\mu}_*}{1 - \bar{\mu}_*}} \,. \tag{72}$$

The damper ratio β_{bif} associated with the bifurcation follows from comparison of the odd-term coefficients, from which the desired damper ratio

$$\bar{\beta} = \bar{\mu}^2 \sqrt{2\,\frac{1 - \bar{\mu}_*}{\bar{\mu}_*}} \tag{73}$$

is obtained by division with $\sqrt{2}$.

From the clamped-mode expansion, the present tuning expressions (71) and (73) contain both the EMCF $\bar{\mu}_*$ and the mass ratio $\bar{\mu}$. For a single-mode structure, the mass ratio equals the EMCF, whereby the root locus diagram and FRF become exactly identical to those from a free-mode expansion in Figs. 5 and 6 for $\bar{\mu} = \bar{\mu}_* = 0.02$. However, for the full flexible structure in Section 6 this will not be the case as residual modes are included, which leads to slightly different results for the tuning with respect to free- and clamped-mode expansions.

5.3. Series inertia absorber: m-[c-k]

This section considers the tuning of the series inertia absorber (m-[c-k]) in Fig. 1(b), for which the damper function is conveniently expressed in reciprocal form as

$$\frac{1}{D(\omega)} = \frac{1}{k} + \frac{1}{i\omega c} \,. \tag{74}$$

The present series inertia absorber m-[c-k] is by construction identical to the corresponding series stiffness absorber k-[c-m] in Fig. 1(d) and Appendix A.2. However, the tuning will not give exactly identical values because the difference in damper element (dashed-blue box) implies a corresponding difference in the residual mode correction by the EMCF.

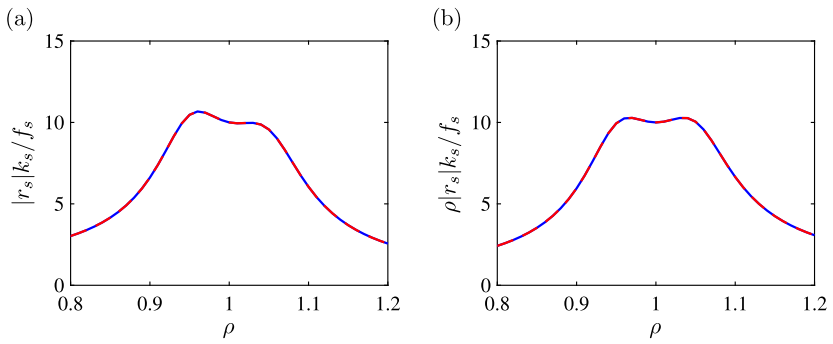

Fig. 7. |FRF| from free-mode expansion: Series inertia absorber (m-[c-k]) with $\mu_* = 0.02$ (blue-solid ——) and series stiffness absorber (k-[c-m]) with $\kappa_* = 0.02$ (red-dashed – –). (a) Modal displacement amplitude $|r_s|$ and (b) modal velocity amplitude $\rho|r_s|$. The modal amplitude is normalized by the static deflection f_s/k_s and ρ is defined in (75).

5.3.1. Free-mode expansion

The frequency response function for the free-mode expansion is determined by substitution of $D(\omega)$ from (74) into the FRF in (36). The single-root solution is for a series absorber reached by $c \to 0$, for which the normalized frequency

$$\rho = \frac{\omega}{\omega_s} \tag{75}$$

gives the desired single root $\rho = 1$ on the real axis, see Fig. 4. Upon introduction of ρ, the FRF in (36) is compactly written as

$$\frac{r_s k_s}{f_s} = \frac{-\rho^2\mu_* + i\rho\dfrac{\mu_*\kappa}{\beta} + \kappa}{\left(1-\rho^2\right)\left(-\rho^2\mu_* + i\rho\dfrac{\mu_*\kappa}{\beta} + \kappa\right) - \rho^2\mu_*\kappa}\,, \tag{76}$$

with the stiffness ratio κ and damper ratio β respectively defined in (47) and (59). The characteristic equation from the denominator can be written in similar form as the generic polynomial in (54), whereby a one-to-one comparison of coefficients determines the desired absorber parameters as

$$\kappa = \mu_*\,, \qquad \beta = \sqrt{\tfrac{1}{2}\mu_*}\,, \tag{77}$$

in which case the damper ratio $\beta = \sqrt{2}\beta_{\text{bif}}$ places the complex roots at the circles on the semi-circular branches in Fig. 4.

Without residual mode correction, the EMCF recovers the mass ratio: $\mu_* = \mu$. In that idealized case, the stiffness tuning in (77) reduces to $\kappa = \mu$, which reflects the inherent equivalence of the two series absorbers in Figs. 1(b) and (d), where spring and inerter can switch positions without altering the absorber characteristics.

In Fig. 7 the modal structural response for the series inertia absorber (m-[c-k]) is represented by the blue-solid curve, while the exactly identical red-dashed curve represents the corresponding series stiffness absorber (k-[c-m]) from Appendix A.2.1. The FRF for the modal displacement $|r_s|$ in Fig. 7(a) is slightly inclined because the tuning is based on equal modal damping, see results in [18,68] for the piezoelectric absorber with a parallel RL-shunt. Thereby, the corresponding velocity amplitude curve ($\rho|r_s|$) in Fig. 7(b) becomes almost ideally flat.

The amplitude curves for the absorber elongations v and $u - v$ are shown in Fig. 8. The damper element elongation v is found from the absorber equation (35) by introducing the absorber force as $f = D(\rho)v$ and ρ from (75),

$$\frac{vk_s}{f_s} = \frac{-\rho^2\mu_*}{-\rho^2\mu_* + D(\rho)/k_s}\,\frac{r_s k_s}{f_s}\,. \tag{78}$$

In Fig. 8(a) the blue-solid curve for v has an ideal flat plateau around resonance. The corresponding inerter elongation $u - v$ is subsequently found by (66), with the absorber function introduced as $G(\rho)/k_s = -\rho^2\mu$. This response curve in Fig. 8(b) exhibits an inclination that makes it flat for the corresponding acceleration amplitude $\rho^2|u - v|$. The red-dashed curves in Fig. 8 represent the series stiffness absorber (k-[c-m]), for which v and $u-v$ are practically interchanged compared to the blue-solid curves for the present inertia absorber. Thereby, the amplitude curve in Fig. 8(b) becomes entirely flat for the elongation $u - v$ across the spring in Fig. 1(d).

5.3.2. Clamped-mode expansion

For the clamped-mode expansion, the frequency response function is obtained by substitution of the damper function $D(\omega)$ from (74) into the clamped-mode FRF in (45). The non-dimensional frequency is then introduced as

$$\bar\rho = \sqrt{1-\bar\mu_*}\,\frac{\omega}{\bar\omega_s} \tag{79}$$

because it secures the desired single-root solution $\bar\rho = 1$ when $c \to 0$. When introducing $\bar\rho$, the FRF in (45) with $D(\omega)$ from (74) can be expressed as

$$\frac{\bar r_s \bar k_s}{\bar f_s} = \frac{(1-\bar\mu_*)\left(-\bar\rho^2\bar\mu + i\bar\rho\dfrac{\bar\mu\bar\kappa}{\bar\beta}\sqrt{1-\bar\mu_*} + \dfrac{\bar\mu_*}{\bar\mu}(1-\bar\mu_*)\bar\kappa\right)}{\left(1-\bar\mu_*-\bar\rho^2\right)\left(-\bar\rho^2\bar\mu + i\bar\rho\dfrac{\bar\mu\bar\kappa}{\bar\beta}\sqrt{1-\bar\mu_*} + \dfrac{\bar\mu_*}{\bar\mu}(1-\bar\mu_*)\bar\kappa\right)\ldots} \\ \frac{}{\ldots + \bar\rho^2\bar\mu_*\left(-\bar\rho^2\bar\mu + i\bar\rho\dfrac{\bar\mu\bar\kappa}{\bar\beta}\sqrt{1-\bar\mu_*}\right)}\,, \tag{80}$$

where the denominator directly defines the characteristic equation, from which the optimal absorber parameters are determined as

$$\bar\kappa = \frac{\bar\mu^2}{\bar\mu_*(1-\bar\mu_*)}\,, \qquad \bar\beta = \bar\mu^2\sqrt{\frac{1}{2\bar\mu_*^3}}\,, \tag{81}$$

by applying the previous one-to-one comparison with the generic polynomial (54).

For the single-dof model with $\bar\mu_* = \bar\mu = 0.02$, the frequency response curves are identical to those from the free-mode expansion, shown in Figs. 7 and 8. However, for a flexible structure, the influence of residual modes ($\bar\mu_* \neq \bar\mu$) implies small differences when using either the free- or clamped-mode expansion, as shown in Section 6. Furthermore, the apparent symmetry ($\kappa = \mu$) between spring and inerter, observed for the free-mode expansion in (77), is not obvious from (81) because the factor $(1 - \bar\mu_*)$ accounts for the presence of the inertance m in the clamped eigenvalue problem (10) and in the auxiliary mass of the mechanical model in Fig. 3(b).

The tuning expressions for the corresponding series stiffness absorber (k-[c-m]) from a clamped-mode expansion are presented in Appendix A.2.2. Because the inertia and stiffness absorbers with series damper elements in Fig. 1(b, d) are identical absorbers, the resulting expressions for optimal tuning are as well identical when interchanging μ and κ.

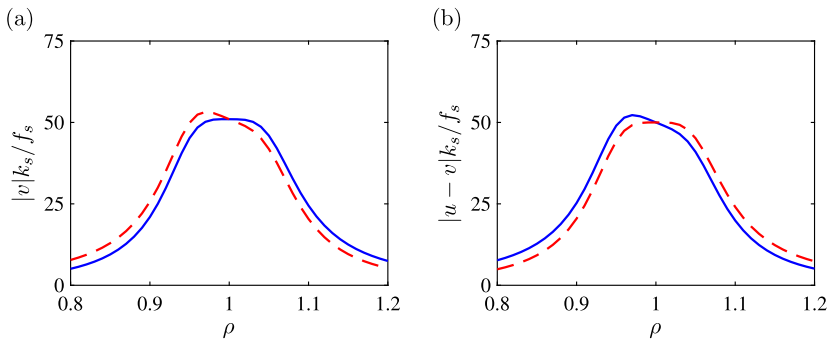

Fig. 8. |FRF| from free-mode expansion: Parallel inertia absorber (m-[c||k]) with $\mu_* = \mu = 0.02$ (blue-solid ——) and parallel stiffness absorber (k-[c||m]) with $\kappa_* = \kappa = 0.02$ (red-dashed – –). (a) Damper element amplitude $|v|$ and (b) absorber element amplitude $|u - v|$. Modal amplitude is normalized by the static deflection f_s/k_s.

6. Damping of flexible structures

The tuning and efficiency of both inertia and stiffness absorbers are assessed with respect to damping of the generic shear-frame structure in Fig. 1, where the horizontal displacements in

$$\mathbf{q}^T = [\, q_1,\, q_2,\, \dots\, q_{10}\,] \tag{82}$$

represent the $n = 10$ dofs of the numerical model. Further details on a shear frame model can be found in [28,35,69]. This numerical model is in general a suitable example to illustrate the influence from residual modes because its frequencies are more closely spaced than those for transverse vibrations of beams.

All absorbers are placed between ground and first floor, whereby the connectivity vector for the shear-frame model is

$$\mathbf{w}^T = [\, 1,\, 0,\, 0,\, \dots\,] \,. \tag{83}$$

As demonstrated in [28,35], this absorber location is optimal with respect to mitigation performance, while it also implies a substantial interaction with the residual modes ($j \neq s$). In case the shear-frame's bottom inter-storey stiffness represents the restoring effects from a base-isolation system, the present absorber location in (83) resembles the seismic protection system proposed by De Domenico et al. [70].

The tuning expressions for the various inertia and stiffness absorbers are collected in Table 1, with the asterisks denoting the respective EMCFs. The expressions for the inertia absorbers in the upper half of the table are derived in the previous Section 5, while the corresponding expressions for the stiffness absorbers in the bottom half are summarized in Appendix A. It is seen that tuning expressions for inertia and stiffness absorbers are identical when interchanging κ and μ.

The next Section 6.1 defines the absorber characteristics in the numerical example, as well as summarizing the tuning procedure in Table 2. The accuracy of the proposed tuning strategy, based on the EMCF, is demonstrated by frequency response curves in Section 6.2 and by a root-locus analysis in the final Section 6.3. All numerical results are computed for the 10-dof shear frame structure in Fig. 1.

6.1. Absorber properties

The tuning of the vibration absorbers is summarized by the steps in Table 2. For the present examples, the size of the inertia and stiffness absorbers is chosen so that their free-mode ratios are $\mu = 0.02$ and $\kappa = 0.02$, respectively. The governing mass and stiffness ratios, and the corresponding EMCFs, are presented for target modes $s = 1$ and 3 in Table 3. EMCFs around 2% correspond well with commonly used mass ratios for TMDs [2,71] and EEMCFs (often referred to as K^2) in piezoelectric shunt damping [1,38–48,57,64]. For inerter-based absorbers, the mass ratio can be increased substantially beyond $\mu = 0.02$, utilizing gearing concepts to mechanically amplify the apparent absorber mass m. For example, in [28,30] inerter mass ratios between 0.1 and 0.2 have been used for structural damping in TIDs. However, to achieve comparable damping performance between inertia and stiffness absorbers, the rather conservative mass ratio $\mu = 0.02$ is chosen also for the inertia absorbers in the present numerical analysis.

For the inertia absorbers, in the left half of Table 3, the free-mode EMCF is slightly larger than the corresponding mass ratio $\mu = 0.02$, whereas for the clamped-mode expansion the EMCFs $\bar{\mu}_*$ are smaller than $\bar{\mu}$. For the stiffness absorbers in the right half of the table, the EMCF to stiffness ratio relations are qualitatively opposite to those for the inertia absorbers.

The difference between the mass or stiffness ratios and their corresponding EMCFs is a direct measure for the influence from residual vibration modes. For the inertia absorbers, the ratios between absorber mass and residual modal mass are given in (33) and (42), with similar expressions available for the associated stiffness absorbers. From these expressions the residual mode ratios can be readily derived as

$$\frac{m_s}{m_s'} = \frac{1}{\mu_*} - \frac{1}{\mu}\,, \quad \frac{\bar{m}_s}{\bar{m}_s'} = \frac{1}{\bar{\mu}} - \frac{1}{\bar{\mu}_*}\,, \quad \frac{k_s}{k_s'} = \frac{1}{\kappa_*} - \frac{1}{\kappa}\,, \quad \frac{\bar{k}_s}{\bar{k}_s'} = \frac{1}{\bar{\kappa}} - \frac{1}{\bar{\kappa}_*}\,, \tag{84}$$

which are as well presented in Table 3. It is seen that the residual mode ratios are negative for inertia absorbers, which reflects that most of the $n - 1 = 9$ residual modes have higher frequency and thereby act statically on the target modes $s = 1$ and 3. However, it is less negative for $s = 3$, since two ($j = 1$ and 2) out of the nine residual modes operate inertially. For the stiffness absorbers in Table 3, the residual mode ratios are consequently positive, with a smaller influence from residual modes for $s = 3$. For even higher target modes, the residual mode ratios in (84) may potentially vanish, whereby the EMCF equals its respective mass or stiffness ratio.

6.2. Frequency response curves

For all absorber configurations, the coupled equations can be rewritten by eliminating the absorber force as in (4). The governing equations can then be expressed in the generic format

$$\left(-\omega^2\mathbf{M}_a + i\omega\mathbf{C}_a + \mathbf{K}_a\right)\mathbf{q}_a = \mathbf{f}_a\,, \tag{85}$$

with the augmented displacement vector $\mathbf{q}_a^T = [\mathbf{q}^T\,, v]$ containing the damper element elongation v as the additional dof, while the load vector $\mathbf{f}_a^T = [\mathbf{f}_{\text{ext}}^T\,, 0]$. The three augmented matrices in (85) are presented for each of the four absorber configurations in Appendix B, which also presents the closed-form expressions for natural frequencies and mode shapes of the n-floor shear frame in Fig. 1. The matrix equation (85) is in the following used to obtain frequency response curves for the top-floor displacement from an external load vector $\mathbf{f}_{\text{ext}} \propto \mathbf{u}_s$ that minimizes any activation of other modes ($j \neq s$).

Fig. 9 shows the frequency response curve for the top-floor velocity amplitude $|i\omega q_{top}|$ with target mode $s = 1$. The curves are all normalized by the pseudo-static amplitude $\omega_1 q_{top}^{stat}$, where q_{top}^{stat} is the top-floor deflection in the static limit ($\omega = 0$). The solid curves represent the proposed tuning, while the dashed curves neglect residual mode

Table 2
Absorber tuning for a given mode $j = s$.

	Inertia		Stiffness
(1) choose modal ratio	$\mu = 0.02$		$\kappa = 0.02$
(2) solve free eigenvalue problem		$\omega_s,\ \mathbf{u}_s,\ m_s,\ k_s$	
(3) determine absorber parameter	$m = \mu m_s$		$k = \kappa k_s$
(4) solve clamped eigenvalue problem		$\bar{\omega}_s,\ \bar{\mathbf{u}}_s,\ \bar{m}_s,\ \bar{k}_s$	
(5) determine clamped-mode ratio	$\bar{\mu} = m/\bar{m}_s$		$\bar{\kappa} = k/\bar{k}_s$
(6) evaluate EMCF	μ_*		κ_*
	or $\bar{\mu}_*$		or $\bar{\kappa}_*$
(7) tune damper parameters	$\kappa,\ \beta$		$\mu,\ \beta$
	or $\bar{\kappa},\ \bar{\beta}$		or $\bar{\mu},\ \bar{\beta}$
(8) determine damper components	$k = \kappa k_s,\ c = \beta\sqrt{k_s m_s}$		$m = \mu m_s,\ c = \beta\sqrt{k_s m_s}$
	or $k = \bar{\kappa}\bar{k}_s,\ c = \bar{\beta}\sqrt{\bar{k}_s \bar{m}_s}$		or $m = \bar{\mu}\bar{m}_s,\ c = \bar{\beta}\sqrt{\bar{k}_s \bar{m}_s}$

Table 3
Mass and stiffness ratios, EMCFs and residual mode ratios.

	m-[c...]		k-[c...]	
Target mode	Free	Clamped	Free	Clamped
$s = 1$	$\mu = 0.0200$	$\bar{\mu} = 0.0235$	$\kappa = 0.0200$	$\bar{\kappa} = 0.0165$
	$\mu_* = 0.0219$	$\bar{\mu}_* = 0.0214$	$\kappa_* = 0.0184$	$\bar{\kappa}_* = 0.0180$
	$m_s/m_s' = -4.34$	$m_s/\bar{m}_s' = -4.18$	$k_s/k_s' = 4.35$	$k_s/\bar{k}_s' = 5.05$
$s = 3$	$\mu = 0.02000$	$\bar{\mu} = 0.0227$	$\kappa = 0.0200$	$\bar{\kappa} = 0.0169$
	$\mu_* = 0.0216$	$\bar{\mu}_* = 0.0211$	$\kappa_* = 0.0186$	$\bar{\kappa}_* = 0.0182$
	$m_s/m_s' = -3.70$	$m_s/\bar{m}_s' = -3.34$	$k_s/k_s' = 3.76$	$k_s/\bar{k}_s' = 4.23$

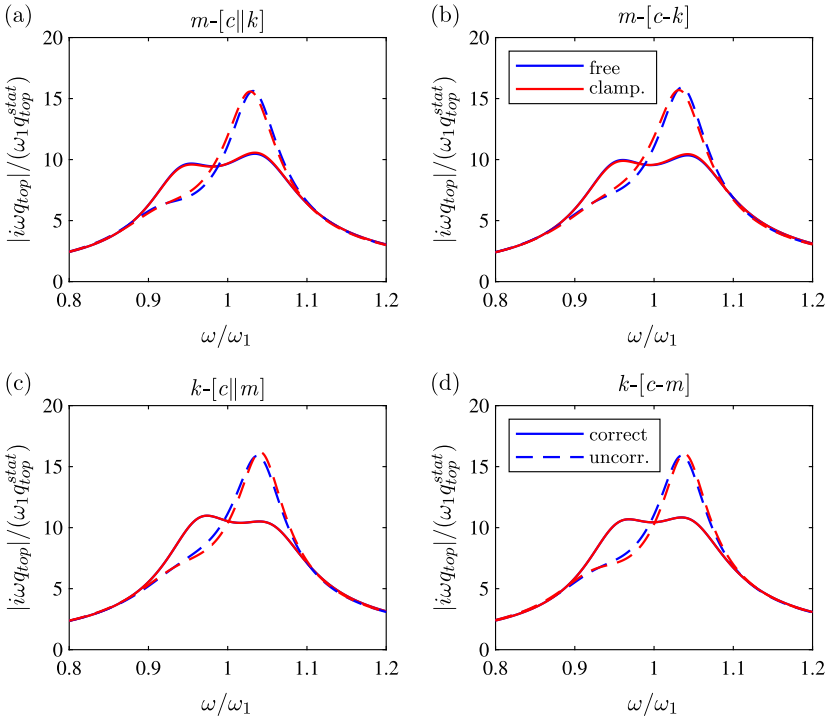

Fig. 9. |FRF| for top floor velocity amplitude $|i\omega q_{top}|$ of shear frame structure. Absorber types: (a) Parallel inertia m-[c||k], (b) series inertia m-[c-k], (c) parallel stiffness k-[c||m] and (d) series stiffness k-[c-m]. Tuning to mode $s = 1$ from free-mode expansion in blue and from clamped-mode expansion in red. Proposed tuning with correction (solid ——) using EMCF and without correction (dashed – –) by EMCF equal to mass ratio (a, b) or stiffness ratio (c, d). Amplitudes normalized by $\omega_1 q_{top}^{stat}$, where q_{top}^{stat} is static top-floor displacement.

correction by replacing any EMCF by its corresponding modal ratio: $\mu_* = \mu$, $\bar{\mu}_* = \bar{\mu}$ in (a, b) for the inertia absorbers and $\kappa_* = \kappa$, $\bar{\kappa}_* = \bar{\kappa}$ in (c, d) for the stiffness absorbers. For the uncorrected tuning (dashed) a substantial amplitude amplification occurs (around 50%). Because of the present tuning procedure's ability to obtain near optimal amplitude reduction at resonance, the very small amplitude increase, which can be seen outside the resonance bandwidth in Fig. 10, is acceptable in engineering practice.

When using the optimal tuning (solid), the |FRF| curves from free-mode (blue) and clamped-mode (red) expansion practically coincide, which demonstrates that the influence from residual modes is consistently accounted for by the proposed tuning with the EMCFs in Table 1. Furthermore, the solid curves in Fig. 9 for the flexible 10-dof structural model almost exactly recover the analytical curves in Figs. 5(c) and 7(b) for parallel and series absorbers, respectively.

The frequency amplitudes for the absorber deflections are shown in Fig. 10. From the previous Figs. 6 and 8 it is seen that a flat plateau is obtained for v by the inertia absorbers, while $u - v$ becomes flat for the stiffness absorbers. Thus, the apparent flatness of the absorber response is observed across the spring element in Fig. 1. The solid

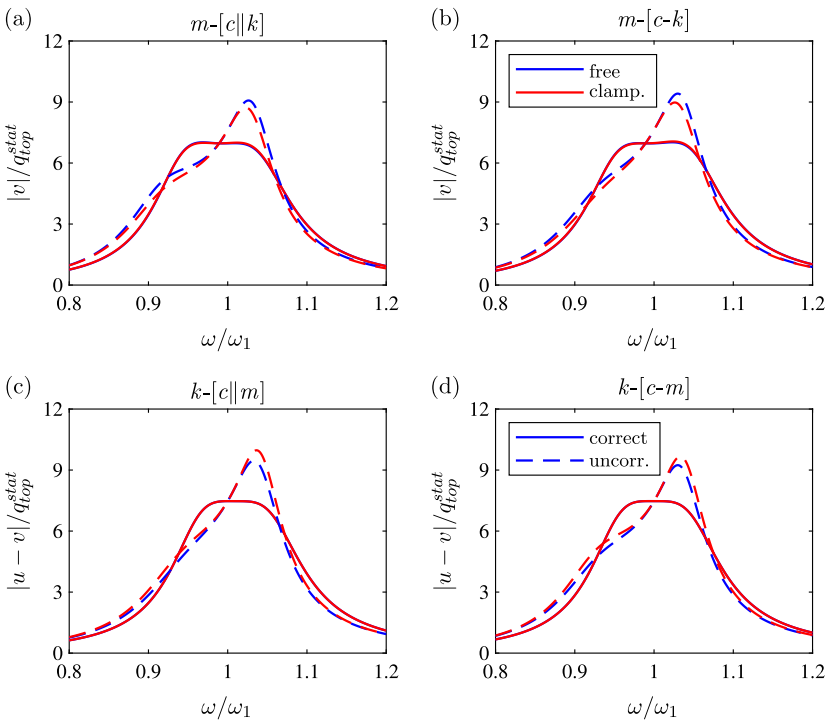

Fig. 10. |FRF| for damper element elongation $|v|$ for (a) parallel inertia m-[c‖k] and (b) series inertia absorber m-[c-k], and absorber element elongation $|u-v|$ for (c) parallel stiffness k-[c‖m] and (d) series stiffness absorber k-[c-m]. Tuning to mode $s=1$ from free-mode expansion in blue and from clamped-mode expansion in red. Proposed tuning with correction (solid ——) using EMCF and without correction (dashed – –) by EMCF equal to mass ratio (a, b) or stiffness ratio (c, d). Amplitudes normalized by static top-floor displacement q_{top}^{stat}.

curves in Fig. 10 for the flexible 10-dof structure model almost exactly replicate the analytical curves in Figs. 6 and 8 for the parallel and series absorbers, respectively. When the EMCF is equal to the corresponding mass or stiffness ratio (dashed) an undesired amplitude amplification is obtained, similar to what is seen for the structural response in Fig. 9.

For the higher target mode $s=3$, the frequency response functions for the inertia absorbers are shown in Fig. 11. A comparison of (a, b) in Figs. 9 and 11 shows that for the proposed tuning, the amplitude curves are almost equally flat, which demonstrates that the EMCF-based tuning is also applicable for intermediate modes ($s>1$). The same conclusions are reached when comparing absorber deflection amplitudes v in the previous Fig. 10(a, b) for $s=1$ and the present Fig. 11(c, d) for $s=3$. The curves for mode $s=3$ with the stiffness absorbers are not presented, as they are practically identical to those for $s=1$ in Figs. 9(c, d) and 10(c, d).

6.3. Root locus curves

The root locus diagrams are produced by solving the state-space eigenvalue problem

$$\begin{bmatrix} \mathbf{0}_a & \mathbf{I}_a \\ -\mathbf{M}_a^{-1}\mathbf{K}_a & -\mathbf{M}_a^{-1}\mathbf{C}_a \end{bmatrix} \begin{bmatrix} \mathbf{q}_a \\ i\omega\mathbf{q}_a \end{bmatrix} = i\omega \begin{bmatrix} \mathbf{q}_a \\ i\omega\mathbf{q}_a \end{bmatrix}, \tag{86}$$

for which the augmented matrices are given in Appendix B. Fig. 12 shows the root locus trajectories for tuning to the fundamental mode $s=1$. The dots along the trajectories are obtained by solving the eigenvalue problem in (86) with respect to $i\omega$ for varying viscous coefficients c in the augmented damping matrix $\mathbf{C}_a$.

The four sub-figures represent the loci for the parallel (a, c) and series (b, d) inertia absorbers, with tuning from a free-mode expansion (blue) and clamped-mode expansion (red). In (a, b) the loci are obtained by the proposed tuning with EMCFs in Table 1, while in (c, d) a detuning is obtained by letting the EMCFs be equal to their respective mass ratios. The corresponding curves for the stiffness absorbers are not presented, as they yield the same qualitative conclusions.

For both inertia absorbers in Fig. 12, the free- and clamped-mode expansions result in practically identical solutions. For the proposed tuning (a, b) the two branches almost meet for $\beta=\beta_{\text{bif}}$ at the desired bifurcation point (∗), previously depicted for the analytical solution in Fig. 5(a). The accuracy of the proposed tuning procedure is further validated by the two desired roots (circle) having practically equal damping, as indicated by the almost coinciding blue and red (dotted) lines from the origin through the blue and red circles, respectively. When neglecting the residual mode correction (c, d), the loci do not approach a bifurcation point, resulting in a small semi-circular trajectory that yields a substantial reduction in attainable damping.

Tables 4 and 5 present the two damping ratios ζ for the two vibration forms associated with the targeted mode $s=1$ and 3, respectively. The damping ratios are evaluated from the roots (∘) obtained for optimal tuning in Table 1 by the procedure in Table 2. Thus accurate tuning should yield a pair of identical damping ratios. The bottom half of the tables present the damping ratios for the stiffness absorbers, for which the root locus diagrams are not presented. The left half of the tables represents tuning based on free-mode expansion, while the right part contains the damping ratios obtained from the tuning expressions based on a clamped-mode expansion. As the free-mode tuning only contains the EMCF (μ_* or κ_*), the corresponding mass or stiffness ratios are not provided.

For both the left and right half of Tables 4 and 5, the first column represents the optimal tuning, while the second column represents the detuning obtained by the EMCF equal to its modal ratio. The first column (for each half in both tables) shows that almost exact equal damping is assured by using the EMCF as depicted by the tuning expressions in Table 1. The largest error of around 8% (0.0426/0.0462 = 0.92) is found for the clamped-mode tuning of m-[c-k] with respect to $s=3$ in Table 5. For the deliberate detuning in the second column, the smallest deviation of around 43% (0.0308/0.0541 = 0.57) between the damping ratios for the free-mode tuning of m-[c‖k] in Table 5 verifies the 50% overshoot observed for the dashed |FRF| curves in Figs. 9 and 11.

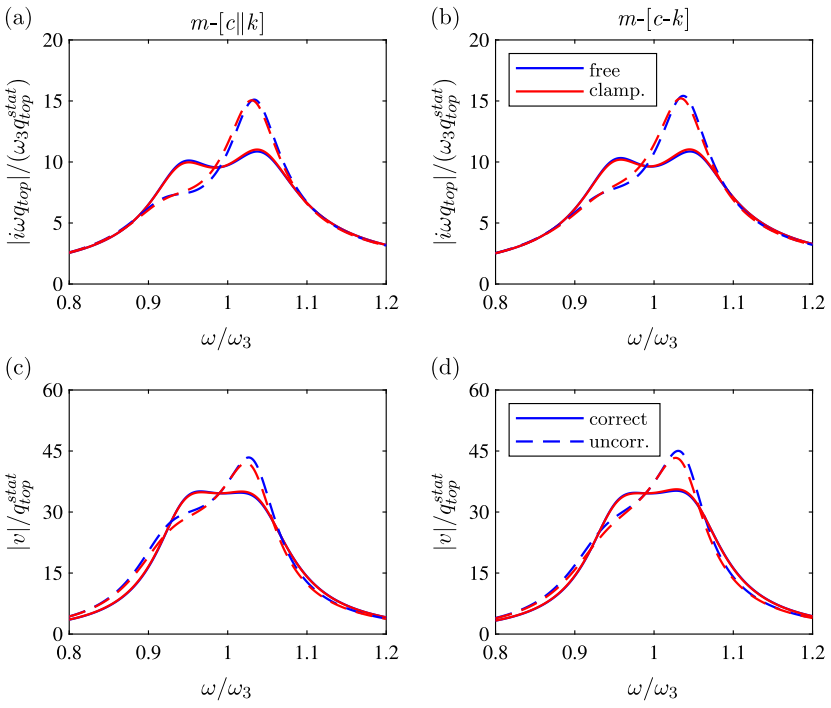

Fig. 11. |FRF| for (a, b) top floor velocity amplitude $|i\omega q_{top}|$ of shear frame structure and (c, d) damper element amplitude $|v|$. Absorber types: (a, c) Parallel inertia m-[c‖k] and (b, d) series inertia m-[c-k]. Tuning to mode $s = 3$ from free-mode expansion in blue and from clamped-mode expansion in red. Proposed tuning with correction (solid ——) using EMCF and without correction (dashed – –) by EMCF equal to mass ratio. Amplitudes normalized by $\omega_3 q_{top}^{stat}$ (a, b) and the static top-floor displacement q_{top}^{stat} (c, d).

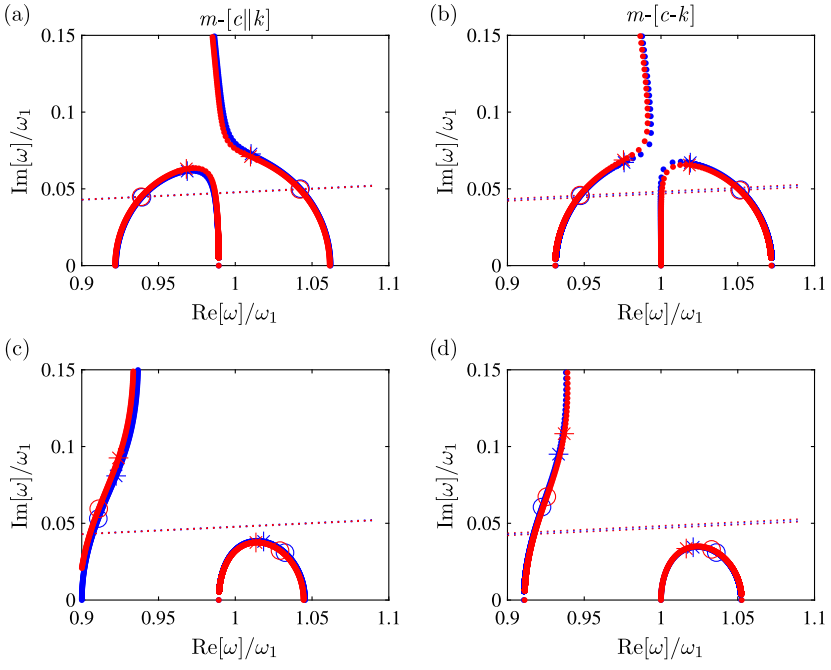

Fig. 12. Root locus diagram for inertia absorbers on shear frame structure: (a, c) Parallel inertia m-[c‖k] and (b, d) series inertia m-[c-k]. Tuning to mode $s = 1$ from free-mode expansion in blue and from clamped-mode expansion in red. Proposed tuning with correction (solid ——) using EMCF in (a, b) and without correction (dashed – –) by EMCF equal to mass ratio in (c, d). Dotted lines represent damping ratio for proposed tuning through circles (∘) in (a, b). Bifurcation tuning represented by asterisks (∗).

By construction the two series absorbers m-[c-k] and k-[c-m] are identical. However, their tuning is different because they are respectively interpreted as inertia and stiffness absorber, with different residual mode correction. Thus, the deviation between the pair of damping ratios for these two series absorbers represents a measure for the consistency of the present tuning procedure and its correction with respect to residual modes. For the damping ratios in Tables 4 and 5, the largest apparent deviation between m-[c-k] and k-[c-m] is around

Table 4
Two damping ratios ζ for target mode $s = 1$.

	Free		Clamped	
	$\mu_* = 0.0219$	$\mu_* = 0.0200$	$\bar{\mu}_* = 0.0214$ $\bar{\mu} = 0.0235$	$\bar{\mu}_* = 0.0235$ $\bar{\mu} = 0.0235$
m-[$c\|\|k$]	0.0473 0.0480	0.0582 0.0299	0.0477 0.0475	0.0651 0.0313
m-[c-k]	0.0479 0.0470	0.0655 0.0298	0.0484 0.0466	0.0726 0.0319
	$\kappa_* = 0.0184$	$\kappa_* = 0.0200$	$\bar{\kappa}_* = 0.0180$ $\bar{\kappa} = 0.0165$	$\bar{\kappa}_* = 0.0165$ $\bar{\kappa} = 0.0165$
k-[$c\|\|m$]	0.0477 0.0476	0.0730 0.0308	0.0477 0.0476	0.0668 0.0285
k-[c-m]	0.0477 0.0477	0.0655 0.0298	0.0476 0.0477	0.0592 0.0283

Table 5
Two damping ratios ζ for target mode $s = 3$.

	Free		Clamped	
	$\mu_* = 0.0216$	$\mu_* = 0.0200$	$\bar{\mu}_* = 0.0211$ $\bar{\mu} = 0.0227$	$\bar{\mu}_* = 0.0227$ $\bar{\mu} = 0.0227$
m-[$c\|\|k$]	0.0447 0.0449	0.0541 0.0308	0.0454 0.0442	0.0594 0.0322
m-[c-k]	0.0454 0.0431	0.0595 0.0305	0.0462 0.0426	0.0646 0.0324
	$\kappa_* = 0.0186$	$\kappa_* = 0.02000$	$\bar{\kappa}_* = 0.0182$ $\bar{\kappa} = 0.0169$	$\bar{\kappa}_* = 0.0169$ $\bar{\kappa} = 0.0169$
k-[$c\|\|m$]	0.0452 0.0438	0.0652 0.0311	0.0449 0.0440	0.0604 0.0289
k-[c-m]	0.0447 0.0445	0.0595 0.0305	0.0444 0.0449	0.0544 0.0289

4% (0.0426/0.0444 = 0.96) for the clamped-mode tuning with target mode $s = 3$. This indicates, that the proposed residual mode accuracy, comprised by the EMCF, is accurate to within a few percent.

7. Conclusions

The present paper proposes a concise tuning procedure for the most basic group of vibration absorbers, targeting a single vibration mode of a flexible structure. The structural response is described by a modal expansion in vibration modes obtained with the absorber in either free or clamped conditions. In the associated absorber equation, the feedback from the non-targeted (residual) modes is represented by a single residual mode function, which is subsequently eliminated by the introduction of the single natural frequency from the opposite – clamped or free – absorber limit. Furthermore, this elimination directly defines an effective modal coupling factor (EMCF), which constitutes a mass ratio for inertia absorbers and a stiffness ratio for stiffness absorbers. The modal frequency response functions (FRF) are then derived for inertia and for stiffness absorbers, from both the free and clamped mode expansions. It is shown that the EMCF directly replaces the absorber's mass or stiffness ratio when using the commonly applied modal expansion in free vibration modes, while the FRF from a clamped-mode expansion contains both EMCF and mass or stiffness ratio in a non-trivial combination.

The target-mode FRF, with the EMCF containing the influence from residual modes, can be used as the basis for any preferred tuning procedure. For the present pole-placement principle, an accurate tuning must secure a bifurcation point in the root locus diagram, while resulting in near optimal flat plateaus for the frequency amplitudes of both structural velocity and absorber elongation. For the 10-dof shear frame structure in the numerical example, the desired damping performance is obtained by the present procedure, using the novel explicit tuning expressions from the pole-placement principle, with the EMCF accounting for the influence from residual modes. When using mass or stiffness ratios instead of the EMCF, the vibration amplitudes increase by 50%, underlining the importance of correctly using the EMCF when relying on analytical tuning expressions derived for an idealized single-mass structure.

Although beyond the scope of the current theoretical analysis, experiments will be needed to validate the postulated importance of representing residual modes by the use of EMCFs. Similarly, the assessment of the tuning procedure with respect to model and method uncertainties would be of great interest. As demonstrated by Trindade et al. [72], an uncertainty in the piezoelectric capacitance translates directly into notable detuning and thus loss of performance. To what degree the present use of EMCFs has more importance than such uncertainties must be investigated through future experimental campaigns.

CRediT authorship contribution statement

Jan Høgsberg: Writing – review & editing, Writing – original draft, Methodology, Formal analysis. **Boris Lossouarn:** Writing – review & editing, Writing – original draft, Methodology. **Jean-François Deü:** Writing – review & editing, Resources, Methodology, Funding acquisition.

Declaration of competing interest

The authors declare that they have no known competing financial interests or personal relationships that could have appeared to influence the work reported in this paper.

Data availability

No data was used for the research described in the article.

Acknowledgement

The financial support of Jan Høgsberg by the Research Council at Cnam is highly appreciated.

Appendix A. Tuning of stiffness absorbers: *k*-[*c*...]

This appendix concerns the tuning of the stiffness absorbers in Fig. 1 (c, d), which are mechanical equivalents to resonantly shunted piezoelectric transducers, for which a vast variety of tuning expressions are available [14–16,18–20,43,46,55,59].

A.1. Parallel stiffness absorber: k-[c||m]

The parallel configuration of the dashpot and inerter in Fig. 1(c) is governed by the damper function

$$D(\omega) = i\omega c - \omega^2 m \,, \tag{87}$$

which represents the mechanical equivalence of a series RL shunt for piezoelectric vibration damping [15].

A.1.1. Free-mode expansion

The FRF from the free-mode expansion is obtained by substitution of (87) into (48). The single-frequency solution is attained in the limit $c \to \infty$, from which the non-dimensional frequency is defined as

$$\rho = \frac{1}{\sqrt{1+\kappa_*}} \frac{\omega}{\omega_s} \,. \tag{88}$$

When introducing ρ, the FRF can be written as

$$\frac{r_s k_s}{f_s} = \frac{-\rho^2(1+\kappa_*)\mu + i\rho\beta\sqrt{1+\kappa_*} + \kappa_*}{\left(1-(1+\kappa_*)\rho^2\right)\left(-\rho^2(1+\kappa_*)\mu + i\rho\beta\sqrt{1+\kappa_*} + \kappa_*\right)\ldots} \tag{89}$$

$$\frac{}{\ldots + \kappa_*\left(-\rho^2(1+\kappa_*)\mu + i\rho\beta\sqrt{1+\kappa_*}\right)} \,,$$

with EMCF κ_* determined in (46), mass ratio μ in (32) and damper ratio β in (59). The characteristic equation is governed by the denominator in (89), from which a one-to-one comparison with the generic polynomial (54) determines the absorber parameters as

$$\mu = \frac{\kappa_*}{(1+\kappa_*)^2} \,, \qquad \beta = \sqrt{2\frac{\kappa_*^3}{(1+\kappa_*)^3}} \,. \tag{90}$$

The |FRF| is shown in Fig. 5(b) by the red-dashed curve. The associated damper element elongation v is subsequently derived from the absorber equation (35),

$$\frac{v k_s}{f_s} = \frac{\kappa_*}{\kappa_* + D(\rho)/k_s} \frac{r_s k_s}{f_s} \,, \tag{91}$$

where $D(\rho)/k_s$ is introduced from (87) with respect to ρ in (88). Subsequently, the spring elongation $u - v$ is obtained from (66) with $G(\rho)/k_s = \kappa$. The absorber elongations v and $u - v$ are both represented by red-dashed curves in Fig. 6.

A.1.2. Clamped-mode expansion

From the clamped-mode expansion, the FRF is obtained by substitution of (87) into (51), which for $c \to \infty$ determines the non-dimensional frequency

$$\bar{\rho} = \frac{\omega}{\bar{\omega}_s} \,. \tag{92}$$

By introduction of $\bar{\rho}$, the FRF can be written as

$$\frac{\bar{r}_s \bar{k}_s}{\bar{f}_s} = \frac{\left(-\bar{\rho}^2\bar{\mu} + i\bar{\rho}\bar{\beta} + \frac{\bar{\kappa}^2}{\bar{\kappa}_*}\right)}{\left(1-\bar{\rho}^2\right)\left(-\bar{\rho}^2\bar{\mu} + i\bar{\rho}\bar{\beta} + \frac{\bar{\kappa}^2}{\bar{\kappa}_*}\right) - \bar{\kappa}^2} \,. \tag{93}$$

The denominator defines the characteristic equation, from which a direct comparison with (54) derives the absorber tuning as

$$\bar{\mu} = \bar{\kappa}^2 \frac{1-\bar{\kappa}_*}{\bar{\kappa}_*} \,, \qquad \bar{\beta} = \bar{\kappa}^2\sqrt{2\frac{1-\bar{\kappa}_*}{\bar{\kappa}_*}} \,. \tag{94}$$

For a single-mode model with $\bar{\kappa}_* = \bar{\kappa}$, the values for c and m from the present clamped-mode expansion tuning recover those obtained from the free-mode expansion in (90).

A.2. Series stiffness absorber: k-[c-m]

The series dashpot-inerter element in Fig. 1(d) is represented by a damper function $D(\omega)$ in the reciprocal relation

$$\frac{1}{D(\omega)} = \frac{1}{-\omega^2 m} + \frac{1}{i\omega c} \,, \tag{95}$$

which is equivalent to the mechanical model of a parallel RL-shunted piezoelectric transducer, see e.g. [20].

A.2.1. Free-mode expansion

The FRF is found by substitution of (95) into (48), which defines the normalized frequency

$$\rho = \frac{\omega}{\omega_s} \tag{96}$$

from the single-root solution when $c \to 0$. The FRF can then be written as

$$\frac{r_s k_s}{f_s} = \frac{-\rho^2\mu + i\rho\frac{\mu\kappa_*}{\beta} + \kappa_*}{\left(1-\rho^2\right)\left(-\rho^2\mu + i\rho\frac{\mu\kappa_*}{\beta} + \kappa_*\right) - \rho^2\mu\kappa_*} \,. \tag{97}$$

When interchanging the asterisk (∗), this FRF is identical to that for the series inertia absorber in (76). Thus, the tuning expressions from (77) can be directly adopted,

$$\mu = \kappa_* \,, \qquad \beta = \sqrt{\tfrac{1}{2}\kappa_*} \,, \tag{98}$$

now with the EMCF κ_* from (46) as the governing parameter. In Fig. 7 the red-dashed curves represent the frequency response curve for r_s from (97). The damper element elongation v is obtained by substitution of (95) into (91), while $u - v$ follows from (66) with $G(\rho)/k_s = \kappa$. The amplitude curves for both absorber elongations (v and $u - v$) are shown in Fig. 8.

A.2.2. Clamped-mode expansion

The FRF is obtained by substitution of the damper function (95) into (51), from which the normalized frequency

$$\bar{\rho} = \frac{1}{\sqrt{1-\bar{\kappa}_*}} \frac{\omega}{\bar{\omega}_s} \tag{99}$$

is determined when $c \to 0$. Hereby, the FRF is expressed as

$$\frac{\bar{r}_s \bar{k}_s}{\bar{f}_s} = \frac{-\bar{\rho}^2(1-\bar{\kappa}_*)\bar{\mu} + i\bar{\rho}\frac{\bar{\mu}\bar{\kappa}}{\bar{\beta}}\sqrt{1-\bar{\kappa}_*}\frac{\bar{\kappa}}{\bar{\kappa}_*} + \frac{\bar{\kappa}^2}{\bar{\kappa}_*}}{\left(1-\bar{\rho}^2(1-\bar{\kappa}_*)\right)\left(-\bar{\rho}^2(1-\bar{\kappa}_*)\bar{\mu} + i\bar{\rho}\frac{\bar{\mu}\bar{\kappa}}{\bar{\beta}}\sqrt{1-\bar{\kappa}_*}\frac{\bar{\kappa}}{\bar{\kappa}_*} + \frac{\bar{\kappa}^2}{\bar{\kappa}_*}\right)\ldots} \tag{100}$$

$$\frac{}{\ldots - \bar{\kappa}\left(i\bar{\rho}\frac{\bar{\mu}\bar{\kappa}}{\bar{\beta}}\sqrt{1-\bar{\kappa}_*} + \bar{\kappa}\right)} \,,$$

from which comparison of the associated characteristic equation with (54) gives

$$\bar{\mu} = \frac{\bar{\kappa}^2}{\bar{\kappa}_*(1-\bar{\kappa}_*)} \,, \qquad \bar{\beta} = \bar{\kappa}^2\sqrt{\frac{1}{2\bar{\kappa}_*^3}} \,. \tag{101}$$

For a single-mode structure with $\bar{\kappa}_* = \bar{\kappa}$, the present tuning gives the same values for c and m as by (98) for the free-mode expansion. Furthermore, the present tuning expressions are similar to those for the series inertia absorber in (81) when interchanging stiffness and mass ratios.

Appendix B. Augmented matrices

The present appendix presents the augmented matrices used in (85) to obtain the frequency response curves (|FRF|) and also used in the homogeneous state-space form (86) as the governing equation for the root locus analysis.

For the n-dof shear frame model in Fig. 2(a), explicit expressions are available for the natural frequencies and mode shapes, see [69] and references herein. They are obtained from the symmetric modes of a vibrating string, spatially discretized by finite differences. For a given mode j, the natural frequency ω_j and mode shape $u_{j,k}$ are given by the expressions

$$\omega_j = 2\sqrt{\frac{k_{storey}}{m_{floor}}}\,\sin\left(\frac{\pi}{2}\frac{2j-1}{2n+1}\right) \,, \quad u_{j,k} = u_{j,0}\sin\left(k\pi\frac{2j-1}{2n+1}\right) \,, \tag{102}$$

where k_{storey} and m_{floor} are respectively the constant inter-storey stiffness and floor mass of the shear frame in Fig. 1, $k = 1, 2 \ldots n$ is the floor number and $u_{j,0}$ is a modal scaling factor that is chosen to secure the desired mode shape normalization.

The four absorber types are shown in Fig. 1, with the two inertia absorbers in (a, b) and the associated stiffness absorbers in (c, d). The matrices are expressed with respect to the augmented displacement vector $\mathbf{q}_a^T = [\mathbf{q}^T, v]$, which combines the structural dofs in $\mathbf{q}$ and the elongation v of the damper element inside the dashed-blue box.

For the parallel inertia absorber m-[$c\|k$] in Fig. 1(a), the augmented matrices are

$$\mathbf{M}_a = \begin{bmatrix} \mathbf{M} & \mathbf{0} \\ -m\mathbf{w}^T & m \end{bmatrix}, \quad \mathbf{C}_a = \begin{bmatrix} \mathbf{0}\mathbf{0}^T & c\mathbf{w} \\ \mathbf{0}^T & c \end{bmatrix}, \quad \mathbf{K}_a = \begin{bmatrix} \mathbf{K} & k\mathbf{w} \\ \mathbf{0}^T & k \end{bmatrix}, \tag{103}$$

where $\mathbf{0}$ is an $n \times 1$ zeros column vector.

For the series inertia absorber m-[c-k] in Fig. 1(b), the augmented matrices are

$$\mathbf{M}_a = \begin{bmatrix} \mathbf{M} + m\mathbf{w}\mathbf{w}^T & -m\mathbf{w} \\ -m\mathbf{w}^T & m \end{bmatrix}, \quad \mathbf{C}_a = \begin{bmatrix} \mathbf{0}\mathbf{0}^T & \mathbf{0} \\ -\frac{mk}{c}\mathbf{w}^T & \frac{mk}{c} \end{bmatrix},$$
$$\mathbf{K}_a = \begin{bmatrix} \mathbf{K} & \mathbf{0} \\ \mathbf{0}^T & k \end{bmatrix}. \tag{104}$$

Considering the augmented mass matrix for such a series inertia absorber, the use of damper elongation v as the additional dof implies that the absorber mass m supplements the structure mass in $\mathbf{M}$.

For the parallel stiffness absorber k-[$c\|m$] in Fig. 1(c), the augmented matrices are

$$\mathbf{M}_a = \begin{bmatrix} \mathbf{M} & m\mathbf{w} \\ \mathbf{0}^T & m \end{bmatrix}, \quad \mathbf{C}_a = \begin{bmatrix} \mathbf{0}\mathbf{0}^T & c\mathbf{w} \\ \mathbf{0}^T & c \end{bmatrix}, \quad \mathbf{K}_a = \begin{bmatrix} \mathbf{K} & \mathbf{0} \\ -k\mathbf{w}^T & k \end{bmatrix}, \tag{105}$$

which correspond to those for the parallel inertia absorber in (105) when interchanging mass and stiffness.

For the series stiffness absorber k-[c-m] in Fig. 1(d), the augmented matrices are

$$\mathbf{M}_a = \begin{bmatrix} \mathbf{M} & \mathbf{0} \\ \mathbf{0}^T & m \end{bmatrix}, \quad \mathbf{C}_a = \begin{bmatrix} \mathbf{0}\mathbf{0}^T & \mathbf{0} \\ -\frac{mk}{c}\mathbf{w}^T & \frac{mk}{c} \end{bmatrix},$$
$$\mathbf{K}_a = \begin{bmatrix} \mathbf{K} + k\mathbf{w}\mathbf{w}^T & -k\mathbf{w} \\ -k\mathbf{w} & k \end{bmatrix}. \tag{106}$$

Although the series absorbers m-[c-k] and k-[c-m] are identical, the mass and stiffness matrices in (104) and (106) are respectively opposite because the damper element elongation v is chosen as the governing absorber variable.

References

[1] Kelley CR, Lopp GK, Kauffman JL. Optimizing piezoelectric material location and size for multiple-mode vibration reduction of turbomachinery blades. J Vib Acoust 2021;143(2):021007.

[2] Elias S, Matsagar V. Research developments in vibration control of structures using passive tuned mass dampers. Annual Reviews in Control 2017;44:129–56.

[3] Li Y, Lombardi L, De Luca F, Farbiarz Y, Blandon JJ, Lara Luis A, et al. Optimal design of inerter-integrated vibration absorbers for seismic retrofitting of a high-rise building in Colombia. Journal of Physics: Conference Series 2019;1264(1):012031.

[4] Ormondroyd J, Den Hartog JP. The theory of the dynamic vibration absorber. Trans ASME 1928;50:9–22.

[5] Brock JE. A note on the damped vibration absorber. J Appl Mech 1946;13(4):A284.

[6] Den Hartog JP. Mechanical vibrations. 4th Edn. McGraw-Hill, New York (Reprint by Dover, New York, 1985); 1956.

[7] Zilletti M, Elliott SJ, Rustighi E. Optimisation of dynamic vibration absorbers to minimise kinetic energy and maximise internal power dissipation. J Sound Vib 2012;331(18):4093–100.

[8] Su N, Chen Z, Xia Y, Bian J. Hybrid analytical H-norm optimization approach for dynamic vibration absorbers. Int J Mech Sci 2023;108796.

[9] Shum KM. Tuned vibration absorbers with nonlinear viscous damping for damped structures under random load. J Sound Vib 2015;346:70–80.

[10] Moheimani SOR. A survey of recent innovations in vibration damping and control using shunted piezoelectric transducers. IEEE Trans Control Syst Technol 2003;11(4):482–94.

[11] Behrens S, Fleming AJ, Reza Moheimani SO. Electromagnetic shunt damping. In: Proceedings 2003 IEEE/ASME international conference on advanced intelligent mechatronics. 2, IEEE; 2003, p. 1145–50.

[12] De Marneffe B, Preumont A. Vibration damping with negative capacitance shunts: theory and experiment. Smart Mater Struct 2008;17(3):035015.

[13] Forward RL. Electronic damping of vibrations in optical structures. Appl Opt 1979;18(5):690–7.

[14] Hagood NW, Von Flotow A. Damping of structural vibrations with piezoelectric materials and passive electrical networks. J Sound Vib 1991;146(2):243–68.

[15] Yamada K, Matsuhisa H, Utsuno H, Sawada K. Optimum tuning of series and parallel LR circuits for passive vibration suppression using piezoelectric elements. J Sound Vib 2010;329(24):5036–57.

[16] Soltani P, Kerschen G, Tondreau G, Deraemaeker A. Piezoelectric vibration damping using resonant shunt circuits: An exact solution. Smart Mater Struct 2014;23(12):125014.

[17] Soltani P, Kerschen G, Tondreau G, Deraemaeker A. Tuning of a piezoelectric vibration absorber attached to a damped structure. J Intell Mater Syst Struct 2017;28(9):1115–29.

[18] Høgsberg J, Krenk S. Balanced calibration of resonant shunt circuits for piezoelectric vibration control. J Intell Mater Syst Struct 2012;23(17):1937–48.

[19] Høgsberg J, Krenk S. Balanced calibration of resonant piezoelectric RL shunts with quasi-static background flexibility correction. J Sound Vib 2015;341:16–30.

[20] Høgsberg J, Krenk S. Calibration of piezoelectric RL shunts with explicit residual mode correction. J Sound Vib 2017;386:65–81.

[21] Krenk S. Frequency analysis of the tuned mass damper. J Appl Mech 2005;72(6):936–42.

[22] Inoue T, Ishida Y, Sumi M. Vibration suppression using electromagnetic resonant shunt damper. J Vib Acoust 2008;130(4):041003.

[23] Auleley M, Thomas O, Giraud-Audine C, Mahé H. Enhancement of a dynamic vibration absorber by means of an electromagnetic shunt. J Intell Mater Syst Struct 2021;32(3):331–54.

[24] Palomera-Arias R, Connor JJ, Ochsendorf JA. Feasibility study of passive electromagnetic damping systems. J Struct Eng 2008;134(1):164–70.

[25] Smith MC. Synthesis of mechanical networks: the inerter. IEEE Trans Automat Control 2002;47(10):1648–62.

[26] Hwang JS, Kim J, Kim YM. Rotational inertia dampers with toggle bracing for vibration control of a building structure. Eng Struct 2007;29(6):1201–8.

[27] Ikago K, Saito K, Inoue N. Seismic control of single-degree-of-freedom structure using tuned viscous mass damper. Earthquake Engineering & Structural Dynamics 2012;41(3):453–74.

[28] Lazar IF, Neild SA, Wagg DJ. Using an inerter-based device for structural vibration suppression. Earthquake Engineering & Structural Dynamics 2014;43(8):1129–47.

[29] Wen YK, Gomez F, Li DX, Spencer, Jr. BF. Generalized optimal design of multiple tuned inerter dampers for control of MDOF structures under stochastic seismic excitation. Structural Control and Health Monitoring 2022;29(1):e2853.

[30] Hu YL, Chen MZQ, Shu Z, Huang LX. Analysis and optimisation for inerter-based isolators via fixed-point theory and algebraic solution. J Sound Vib 2015;346:17–36.

[31] Sun HX, Zuo L, Wang XY, Peng J, Wang WX. Exact H_2 optimal solutions to inerter-based isolation systems for building structures. Structural Control and Health Monitoring 2019;26(6):e2357.

[32] Marian L, Giaralis A. Optimal design of a novel tuned mass-damper–inerter (TMDI) passive vibration control configuration for stochastically support-excited structural systems. Probabilistic Engineering Mechanics 2014;38:156–64.

[33] Barredo E, Rojas GL, Mayén J, Flores-Hernández AA. Innovative negative-stiffness inerter-based mechanical networks. Int J Mech Sci 2021;205:106597.

[34] Chowdhury S, Banerjee A, Adhikari S. The optimal design of negative stiffness inerter passive dampers for structures. Int J Mech Sci 2023;108551.

[35] Krenk S, Høgsberg J. Tuned resonant mass or inerter-based absorbers: unified calibration with quasi-dynamic flexibility and inertia correction. Proceedings of the Royal Society A: Mathematical, Physical and Engineering Sciences 2016;472(2185):20150718.

[36] Krenk S. Resonant inerter based vibration absorbers on flexible structures. J Franklin Inst 2019;356(14):7704–30.

[37] Chen B, Zhang Z, Hua XG. Equal modal damping-based optimal design of a grounded tuned mass-damper-inerter for flexible structures. Structural Control and Health Monitoring 2022;29(12):e3106.

[38] Benjeddou A. Modal effective electromechanical coupling approximate evaluations and simplified analyses: numerical and experimental assessments. Acta Mech 2014;225(10):2721–42.

[39] Deü JF, Benjeddou A. Free-vibration analysis of laminated plates with embedded shear-mode piezoceramic layers. Int J Solids Struct 2005;42(7):2059–88.

[40] Ducarne J, Thomas O, Deü JF. Placement and dimension optimization of shunted piezoelectric patches for vibration reduction. J Sound Vib 2012;331(14):3286–303.

[41] Porfiri M, Maurini C, Pouget J. Identification of electromechanical modal parameters of linear piezoelectric structures. Smart Mater Struct 2007;16(2):323–31.
[42] Thomas O, Deü JF, Ducarne J. Vibrations of an elastic structure with shunted piezoelectric patches: efficient finite element formulation and electromechanical coupling coefficients. Internat J Numer Methods Engrg 2009;80(2):235–68.
[43] Thomas O, Ducarne J, Deü JF. Performance of piezoelectric shunts for vibration reduction. Smart Mater Struct 2012;21(1):015008.
[44] Lossouarn B, Aucejo M, Deü JF, Multon B. Design of inductors with high inductance values for resonant piezoelectric damping. Sensors and Actuators A: Physical 2017;259:68–76.
[45] Darleux R, Lossouarn B, Deü JF. Passive self-tuning inductor for piezoelectric shunt damping considering temperature variations. J Sound Vib 2018;432:105–18.
[46] Toftekær JF, Benjeddou A, Høgsberg J. General numerical implementation of a new piezoelectric shunt tuning method based on the effective electromechanical coupling coefficient. Mech Adv Mater Struct 2020;27(22):1908–22.
[47] Lossouarn B, Rouleau L, Darleux R, Deü JF. Comparison of passive damping treatments based on constrained viscoelastic layers and multi-resonant piezoelectric networks. Journal of Structural Dynamics 2021;1.
[48] Lossouarn B, Kerschen G, Deü JF. An analogue twin for piezoelectric vibration damping of multiple nonlinear resonances. J Sound Vib 2021;511(116323):116323.
[49] Basak S, Raman A, Garimella SV. Dynamic response optimization of piezoelectrically excited thin resonant beams. J Vib Acoust 2005;127(1):18–27.
[50] Caruso G. A critical analysis of electric shunt circuits employed in piezoelectric passive vibration damping. Smart Mater Struct 2001;10(5):1059–68.
[51] Deü JF, Larbi W, Ohayon R, Sampaio R. Piezoelectric shunt vibration damping of structural-acoustic systems: Finite element formulation and reduced-order model. J Vib Acoust 2014;136(3).
[52] Giaralis A, Marian L. Use of inerter devices for weight reduction of tuned mass-dampers for seismic protection of multi-story building: the tuned Mass-Damper-Interter (TMDI). In: Park Gyuhae, editor. Active and Passive Smart Structures and Integrated Systems. 9799, SPIE; 2016, p. 415–24.
[53] Hoffmeyer D, Høgsberg J. Calibration and balancing of multiple tuned mass absorbers for damping of coupled bending-torsion beam vibrations. J Vib Acoust 2020;142(4):044501.
[54] Neubauer M, Oleskiewicz R, Popp K, Krzyzynski T. Optimization of damping and absorbing performance of shunted piezo elements utilizing negative capacitance. J Sound Vib 2006;298(1–2):84–107.
[55] Berardengo M, Thomas O, Giraud-Audine C, Manzoni S. Improved resistive shunt by means of negative capacitance: new circuit, performances and multi-mode control. Smart Mater Struct 2016;25(7):075033.
[56] Neubauer M, Han X, Schwarzendahl SM. Enhanced switching law for synchronized switch damping on inductor with bimodal excitation. J Sound Vib 2011;330(12):2707–20.
[57] Raze G, Dietrich J, Lossouarn B, Kerschen G. Shunts vs networks: tuning and comparison of centralized and decentralized piezoelectric vibration absorbers. Smart Mater Struct 2022;31(11):115006.
[58] Krenk S, Høgsberg J. Tuned mass absorber on a flexible structure. J Sound Vib 2014;333(6):1577–95.
[59] Berardengo M, Thomas O, Giraud-Audine C, Manzoni S. Improved shunt damping with two negative capacitances: An efficient alternative to resonant shunt. J Intell Mater Syst Struct 2017;28(16):2222–38.
[60] Clark RL. Accounting for out-of-bandwidth modes in the assumed modes approach: Implications on colocated output feedback control. Journal of Dynamic Systems, Measurement and Control 1997;119(3):390–5.
[61] Moheimani SOR. Minimizing the effect of out of bandwidth modes in truncated structure models. Journal of Dynamic Systems, Measurement and Control 2000;122(1):237–9.
[62] Behrens S, Fleming AJ, Moheimani SOR. A broadband controller for shunt piezoelectric damping of structural vibration. Smart Mater Struct 2003;12(1):18–28.
[63] Halim D, Moheimani SOR. Reducing the effect of truncation error in spatial and pointwise models of resonant systems with damping. Mechanical systems and signal processing 2004;18(2):291–315.
[64] Berardengo M, Manzoni S, Høgsberg J, Vanali M. Vibration control with piezoelectric elements: The indirect measurement of the modal capacitance and coupling factor. Mech Syst Signal Process 2021;151(107350):107350.
[65] Wu SY. Piezoelectric shunts with a parallel R-L circuit for structural damping and vibration control. In: Johnson Conor D, editor. Smart Structures and Materials 1996: Passive Damping and Isolation. 2720, SPIE; 1996, p. 259–69.
[66] Barredo E, Blanco A, Colín J, Penagos VM, Abúndez A, Vela LG, et al. Closed-form solutions for the optimal design of inerter-based dynamic vibration absorbers. Int J Mech Sci 2018;144:41–53.
[67] Krenk S, Høgsberg J. Equal modal damping design for a family of resonant vibration control formats. J Vib Control 2013;19(9):1294–315.
[68] Høgsberg J. Consistent frequency-matching calibration procedure for electromechanical shunt absorbers. J Vib Control 2020;26(13–14):1133–44.
[69] Høgsberg JR, Krenk S. Linear control strategies for damping of flexible structures. J Sound Vib 2006;293(1–2):59–77.
[70] De Domenico D, Impollonia N, Ricciardi G. Soil-dependent optimum design of a new passive vibration control system combining seismic base isolation with tuned inerter damper. Soil Dyn Earthq Eng 2018;105:37–53.
[71] Elias S, Matsagar V, Datta TK. Along-wind response control of chimneys with distributed multiple tuned mass dampers. Structural Control and Health Monitoring 2019;26(1):e2275.
[72] Trindade MA, Lossouarn B, Deü JF. Effect of parametric uncertainties on vibration mitigation with periodically distributed and interconnected piezoelectric patches. J Intell Mater Syst Struct 2021;32(9):971–85.